Climatic and environmental changes during the transition from the Penultimate Glaciation into the Last Interglacial (MIS 6 - 5e): a case study from Niederweningen, Switzerland

Master's Thesis

Faculty of Science

University of Bern

presented by

Andreas Züger

2010

Supervisor:
PD Dr. Frank Preusser
Institute of Geological Sciences and Oeschger Centre for Climate Change Research

Co-Supervisor:
Prof. Dr. Flavio Anselmetti
Swiss Federal Institute of Aquatic Sciences and Technology (EAWAG)

Advisor:
Prof. Dr. Christian Schlüchter
Institute of Geological Sciences and Oeschger Centre for Climate Change Research

Abstract

A 93.6 m deep sediment core NW09 was drilled in Niederweningen in the Wehntal, Northern Switzerland, providing deep insights into the Quaternary environmental history of the last ~260 ka. As the knowledge of the climatic and environmental conditions for the time preceding the Eemian Interglacial (Marine Isotope Stage MIS 5e) is still limited for the Swiss lowlands, this study contributes to advances in the present state of knowledge. The main focus is on the extent of Alpine glaciers during the Penultimate Glaciation (MIS 6) and the climatic and environmental conditions during the transition from MIS 6 into MIS 5e. Geochemical and geophysical methods and a chronology based on luminescence dating revealed information about environmental conditions during the deposition of the sediment. Above a sequence of molasse and basal till at the bottom of the core, a sequence of lacustrine clays with dropstones from MIS 8 was observed, being an indicator for the presence of a proglacial lake in the Wehntal. Followed by a section of lacustrine clays without dropstones covering the entire MIS 7, the luminescence ages revealed a time gap for most of the MIS 6 glacial. This gap is interpreted as a possible glacier advance during MIS 6, as proposed from other sites in the Swiss Midlands. The sediment sequence representing the transition from MIS 6 into MIS 5e is characterised by a decrease in carbonate content (from ~45 to 17 wt-%) and units with increased grain-size (from clayey silt to fine sand). The decreasing carbonate content is probably associated with a change in the catchment area of the glacier due to changing climatic conditions. Moreover, the occurrence of wood fragments and increasing organic carbon content immediately below the Eemian peat indicate a gradual enhancement of the climatic conditions towards MIS 5e, followed by a silting up of the lake and the formation of the peat horizon. A detailed chronology of the transition, however, was not possible, as results from palynological analysis revealed a hiatus at the beginning of the peat horizon.

Contents

List of figures

List of tables

1 Introduction

In March 2009, a 93.6 m long sediment core was taken in Niederweningen, a village situated in the Wehntal, Switzerland. This sediment core "NW09" is the object of research of the Niederweningen project 2009/2010 in which this master thesis is integrated. Besides a general introduction into the research context, the first chapter covers a detailed problem description including the main research questions.

1.1 General context and motivation

The climatic conditions in Switzerland and Central Europe are to a large extent influenced by the presence of the Alps. Today, the Alps separate moderate all-year humid climate conditions to the north and warmer Mediterranean climate to the south. Nevertheless, completely different climatic conditions were present in Europe during glacial times due to different atmospheric circulation patterns and an associated southward shift of the polar front (Florineth and Schlüchter, 2000). Therefore, the Alps and its forelands are interesting areas for paleoclimatic investigations. In addition to the atmospheric impact, the Swiss Alpine Foreland was strongly influenced by Quaternary glaciations. Advancing glaciers led to massive bedrock erosion and re-deposition of unconsolidated sediment, forming different glacial landforms such as glacial basins or moraine ridges (Ehlers, 1996; Anselmetti et al., in press). It is known that several paleo-valleys have been deeply incised into the molasse bedrock of the Swiss Alpine Foreland by such glacial activities (Jordan et al. 2008). The sediment fillings of these so-called overdeepened valleys, such as the Wehntal, contain important information about the environmental conditions during the time of deposition. The analysis of the NW09 core, reaching down to the molasse bedrock, may lead to a better understanding of environmental evolution in the course of the Quaternary and probably provide important information about formation processes of such glacial overdeepened valleys. The Niederweningen project 2009/2010 is mainly being conducted by members of the Paleontological Institute and Museum of the University of Zurich, the Eawag (Swiss Federal Institute of Aquatic Science and Technology) and the Institute of Geological Sciences of the University of Bern.

The motivation to write a master thesis dealing with this topic was manifold. Writing a thesis in the field of luminescence dating was the basic idea. With the introduction to the current Niederweningen project, the multidisciplinarity and the variety of different methods applied to the project have aroused the interest to this project even more. Further, the very limited knowledge of pre-Eemian climate conditions north

of the Alps represents a challenge and additional motivation. The basic motivation, however, is to link the two subjects of climate sciences and geology. As today climate sciences are more present in political and social life than ever before, doing research work in this topic is very interesting and challenging. Climate models are in great demand and are taken into account for environmental- and energy-policy decisions. The basis of climate models is the knowledge of what happened in the past or in the words of a paleoclimatologist: the past is the key to the future. Hence, the link between climate sciences and geology is evident. This project investigates one of the most extensive and accessible of the various geological archives: lake sediments. The subject of lake sediment investigation is known as paleolimnology and addresses for example to the timing of past climate change, rates of evolutionary change in species and the timing of pollutant introduction into watersheds (Cohen, 2003). Hence, the combination of paleolimnological methods and luminescence dating is suited for gaining new insights into past glacial history.

1.2 Thesis' research questions

As most of the previous research was done on the transition from the last glacial cycle into the Holocene (e.g. Amman et al., 1994; Kerschner and Ivy-Ochs, 2008), very little is known about the period preceding the last glaciation and particularly for Eemian (~114 – 125 ka, Bassinot et al., 1994) and pre-Eemian times. Therefore, this thesis will focus on the transition from MIS (Marine Isotope Stage) 6 to 5e, which reflects the transition from the Penultimate Glaciation into the Last Interglacial (Fig. 3-1).

The research focus of this thesis is on the climatic and environmental evolution afore and during the transition into the Eemian interglacial. As mentioned above, the knowledge about pre-Eemian climate evolution and the presence or absence of glaciers is still rather limited and contradictory discussed in literature (e.g. Litt et al., 2007; Habbe, 2007; Schlüchter, 1988a) (compare chapter 3.2). Results from the NW09 core, however, may contain important data about climate change from a glacial into an interglacial and may contribute to a better understanding of this process. The extent of the glaciers and their climatic conditions associated are a possible source of information addressing this problem. As the NW09 core mostly consists of proglacial lake sediments, it contains data about the evolution of such a glacier. To reconstruct the timing of different glacier advances and retreats, the age determination of the sediment is a further relevant objective. The main focus is therefore made up of two research topics: glacier fluctuations and derivation of climate variables on the one hand and temporal evolution and type of climate change on the other hand.

Possible conclusions can only be drawn in consideration of both of these topics.

1.2.1 Glacier fluctuations and derivation of climate variables

The appearance of today's landscape and topography was highly influenced by the presence of Quaternary glaciers and their fluctuations (Anselmetti et al., in press). Moreover, the reduction of Alpine glaciers in the course of the last 150 years showed the high sensitivity of glaciers to climate changes, particularly to changes in temperature (Häberli et al., 2001). Therefore, contributing to a better understanding of the Swiss and European climatic conditions by means of the analysis of the related glaciation history is one objective of the thesis. A special focus is on the presence and extent of glacier advances during the MIS 6 cold period in the Swiss midlands. For this reason, the NW09 core was analysed using different geochemical and geophysical methods.

1.2.2 Temporal evolution and patterns of climate change

Besides the information concerning the mode glaciers fluctuated during glacials and interglacials, there is one essential variable missing for the detection of the temporal evolution of climate change: the age of the sediment. Several issues related to the temporal evolution are part of the main research questions of this thesis. The timing and velocity of the transition from MIS 6 into MIS 5, from initial indicators until the full expansion of the Eemian interglacial, is one task. These findings may lead to a subsequent, more general question dealing with the transition from a glacial into an interglacial. Such a transition has been investigated in detail for the time period from the last glacial (MIS 2 or Würmian) into the present interglacial (MIS 1 or Holocene). Hence, knowledge of this younger transition could be very helpful for the interpretation. In this context, a further issue to investigate is the incidence of a rapid cooling event in the initial phase of the warm period comparable to the 'Younger Dryas' cooling in the beginning of the Holocene ~12,000 years ago. The presence of such a cooling event in the NW09 core would support some propositions in literature (e.g. Sarnthein and Tiedemann, 1990; Seidenkrantz, 1993; Sànchez Goñi et al., 2000) stating it as a general phenomenon during a glacial-interglacial transition. Another objective is to detect proxies, which contain information about trigger mechanisms for the climate change between MIS 6 and 5e. A final objective is related to the methodological part. In this study, the dating of the sediment was conducted using luminescence dating. As there are still some methodological uncertainties concerning the reliability of luminescence dating prior to the Eemian (e.g. Lowick et al., 2010; Murray et al., 2008), a comparison of the dating results with other data from the

NW09 core including temporal information such as pollen analysis could contribute to this discussion.

To summarise, the main research questions are the following:

- Was the research area covered with ice during the MIS 6 and how far did the Alpine glaciers then advance into the Swiss Alpine Foreland?

- When and how fast did the transition from MIS 6 to 5e occur in the Swiss Alpine Foreland?

- Is there evidence for a Younger Dryas - type cooling during the transition to the Eemian interglacial (MIS 5e)?

- Does luminescence dating provide reliable ages for the entire NW09 core?

2 Research area

For the interpretation of a sediment core, the understanding of the surrounding geographical, geological and climatic conditions are essential. The following chapter describes the most important characteristics of the research area and its catchment.

2.1 Geographical and geological setting

The Wehntal is an east-west-oriented valley in the Swiss Midlands about 20 km northwest of Zurich. The drill site is situated in Niederweningen, a village 505 meters above sea level, at the northwestern border of the Canton of Zurich. The borehole was drilled about 160 meters southwest of the Niederweningen train station in the Schnötenstrasse (Swiss Grid coordinates: 670.945 / 261.960) (Fig. 2-1). The recent drainage of the Wehntal is controlled by the brook Surb, having its source in Oberweningen, flowing westwards through Niederweningen and finally discharging into the river Aare at Döttingen.

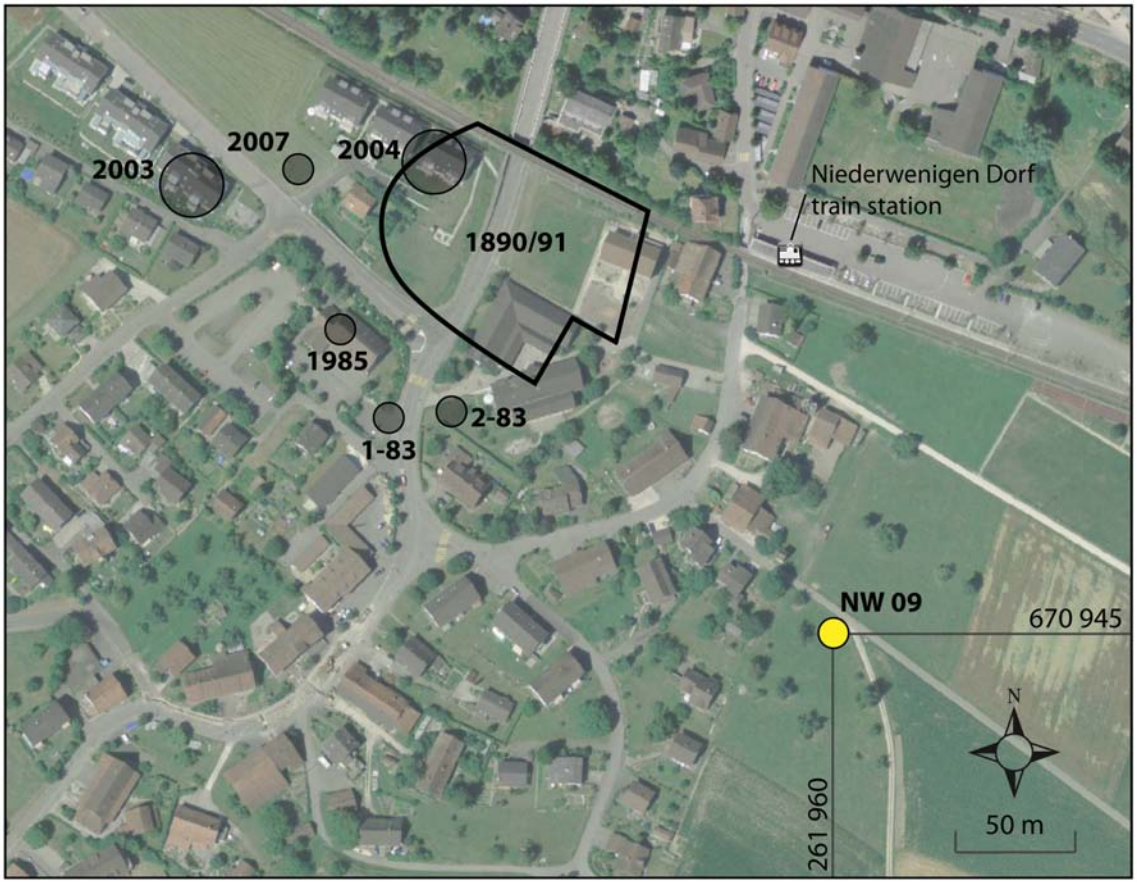

Figure 2-1: Map of Niederweningen with the position of the mammoth pit from 1890/91, the coreholes from 1983 (1-83, 2-83), 1985 and 2007, the construction pits 2003 and 2004 and the drilling location of the Niederweningen project 2009/2010 (NW09). Source: Picture from Google Earth (version 4.3).

The hydrological conditions in particular have changed to a great extent during the Quaternary. Not only glacial activity has influenced the area around Niederweningen, but also the melting of glacier ice, which led to the formation of a large proglacial lake capturing the entire valley and most probably parts of the Glatttal and the area of Lake 'Greifensee' further to the south-east. This proglacial lake caused a filling of the valley with lake sediments, as previous drillings already revealed (e.g. Welten, 1988; Schlüchter, 1988b; Furrer et al., 2007).

The most conspicuous geological element in the Wehntal is the Lägern anticline, forming the southern slope of the Wehntal (Fig. 2-2). The Lägern is part of the Jura Mountains and was formed during the last period of the Alpine folding in Late Miocene to Pliocene (~6-2 Ma ago) and consists mainly of Upper Jurassic limestone (Labhart, 2005).

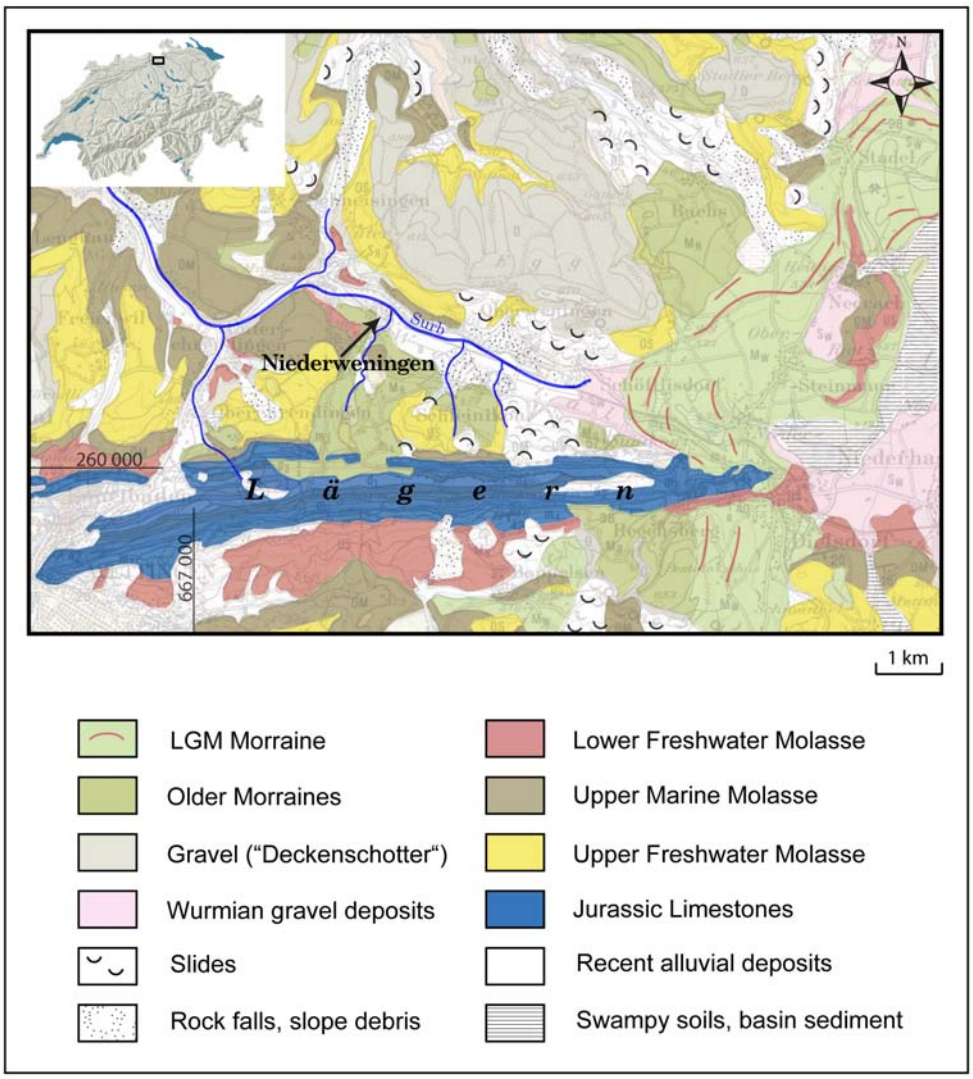

Figure 2-2: Simplified geologic map of the Wehntal including the position of Niederweningen and the main drainage system. Coordinates are indicated in Swiss grid. Source: Inset modified from Atlas der Schweiz 2.0; map modified from Swisstopo, Geologische Karte der zentralen Nordschweiz, 1:100 000.

The recent valley floor is covered with alluvial deposits and the northern slope of the valley is made up of Tertiary Molasse bedrock, partially being covered by the 'Deckenschotter' (Cover Gravel) unit. During the deposition of these gravel in the Early Pleistocene, a precursor of the Wehntal already existed (Furrer et al., 2007). The development of the valley to the present size and the overdeepening below its actual level into the Molasse bedrock was forced by Middle Pleistocene glaciers, but the timing of the formation of the basin is still unknown (Furrer et al. 2007). The terminal moraine ridge at Steinmaur, situated at the valley entrance 4km east of Niederweningen (Fig. 2-2), indicates the maximum ice advance of the Linth-Rhein glacier into the Glatt valley during the Last Glacial Maximum (LGM, around 23 ka) (Keller and Krayss, 2005; Wyssling, 2008) (Fig. 2-3). As a consequence, the entire Wehntal was ice-free during the LGM, leading to the opportunity to reconstruct the glacial history prior to the LGM (Anselmetti et al., in press).

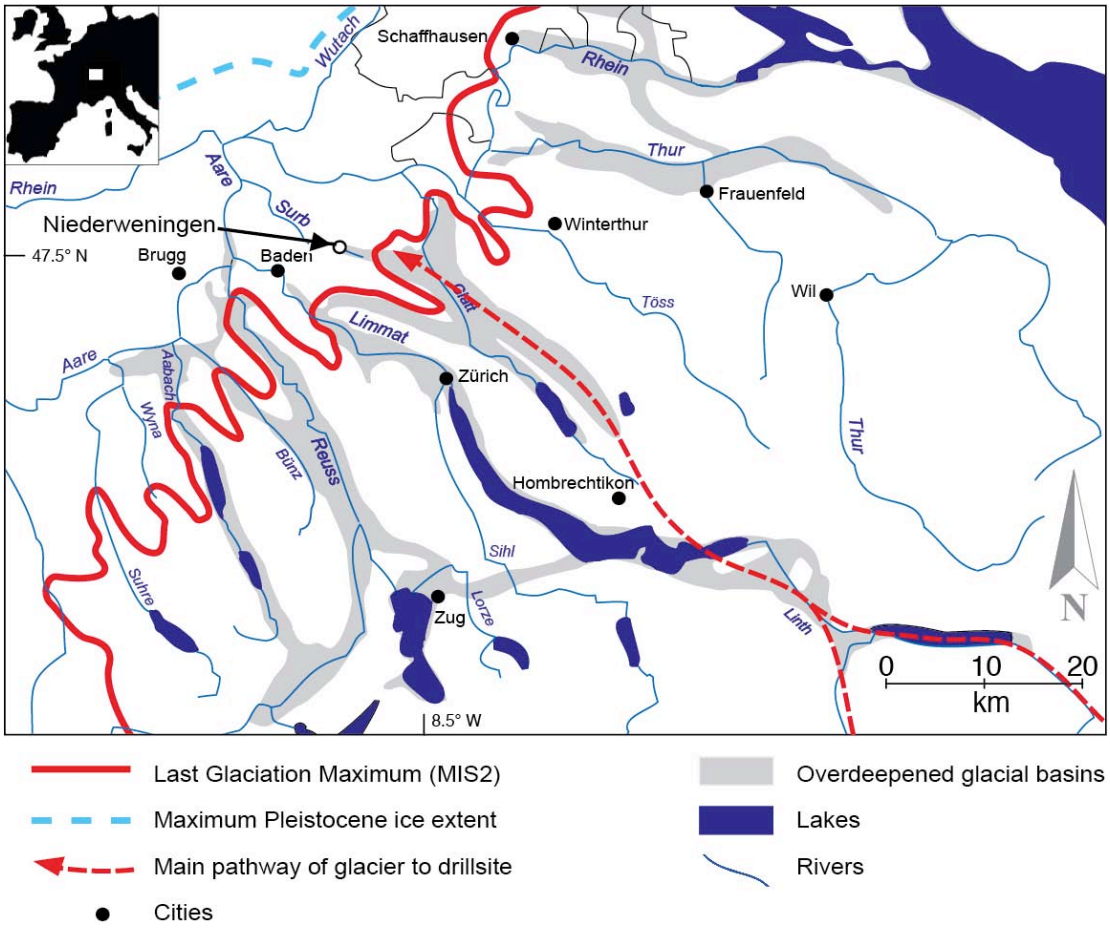

Figure 2-3: Maximum ice extent of the Last Glaciation (MIS 2) and the Most Extensive Pleistocene Glaciation including the main pathway of the glaciers to the drill site of NW09. Source: Anselmetti et al. (in press).

2.2 Recent Climate

Considering the present climate of Europe, there is one dominant pattern: the North Atlantic circulation (Martyn, 1992). Direct manifestations of this influence are the Northern Hemisphere westerlies (Florineth and Schlüchter, 2000). The shifting and meandering course of the westerlies is the leading circulation pattern for mid- to high-latitudes. The core of the westerlies is the polar front jet stream located at approximately 500 hPa (~5.5 km above sea level) (Harrison et al., 1992). Its strength and position vary during the course of the year in response to the seasonal variations of the latitudinal temperature gradient (Florineth and Schlüchter, 2000). Hence, the jet stream moves southwards with an increased strength in winter and polewards with a decreased strength in summer (Harrison et al., 1992). Owing to this occurrence, the influence of the westerlies on Swiss climate is much stronger in winter than in summer. Another important impact on European climate is represented by the Alps. Due to their position between the Mediterranean region and central Europe they amplify the general climatic gradient and act as a climate and weather divide (Florineth and Schlüchter, 2000).

With its position in the Swiss Midlands, the climate in the Wehntal is mainly dominated by westerly winds being channelized through the Alps and the Jura Mountains and bringing mild and humid air masses. A further dominant wind pattern in the Swiss Midlands is the cold and dry continental wind coming from the northeast, known as the Bise (Fig. 2-4). These conditions lead to an average annual precipitation amount of 1031 mm per year and an average annual temperature of 8.5 °C at the Zürich-Kloten weather station 13 km to the east of Niederweningen (MeteoSchweiz, 2010). The highest precipitation amount and temperatures occur during the summer months (Fig. 2-5).

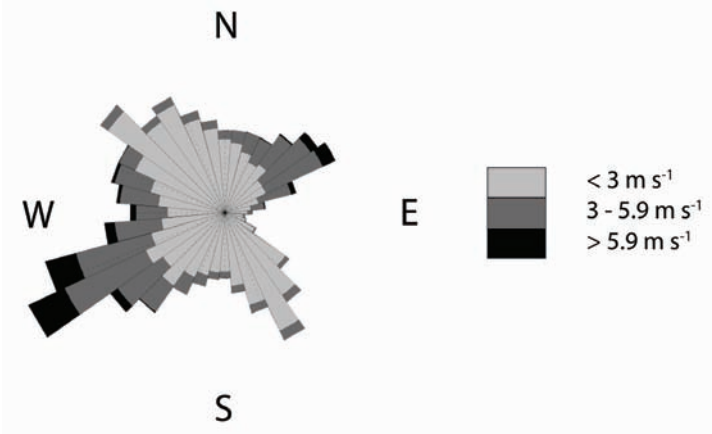

Figure 2-4: Wind rose indicating the most dominant wind patterns at the Zurich-Kloten weather station in the Swiss Midlands 13 km east of Niederweningen. Reference period: 1981-2000. Source: MeteoSchweiz (2010).

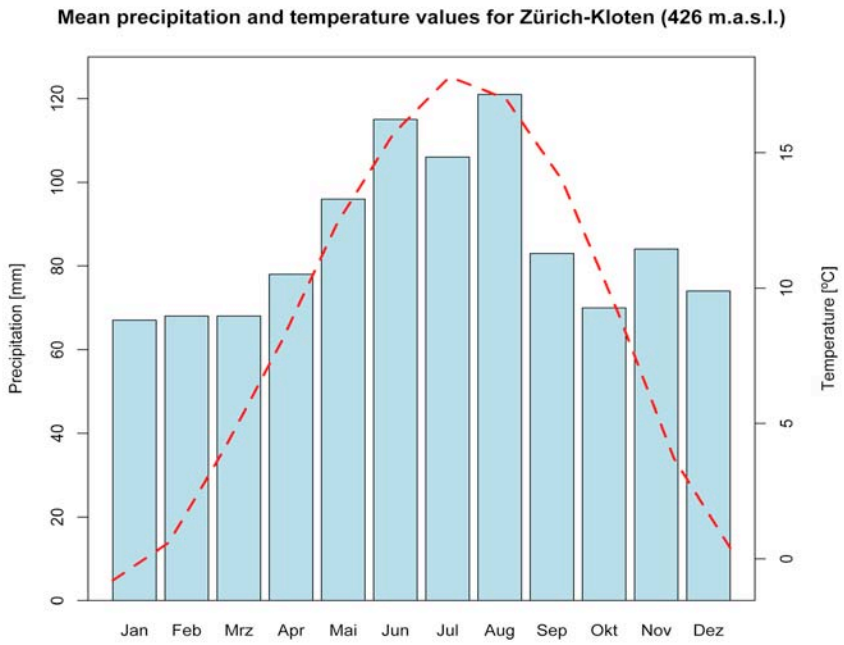

Figure 2-5: Monthly precipitation and temperature values for Zürich-Kloten, 13 km to the east of Niederweningen for the reference period 1961-1990. Data source: Meteoschweiz (2010).

3 State of research

As mentioned above, the ongoing Niederweningen project was preceded by several other projects in the Wehntal. In the following chapter, a chronology of these investigations will be given including the most important scientific findings. This will help to get an overview of the topic and provides an explanation for the selections of the main research topics for the current project. The second part of the chapter deals with the climatic aspects of the problem setting, namely with the climatic conditions during MIS 6 and the transition from MIS 6 to 5e.

3.1 Previous Niederweningen projects

Niederweningen is Switzerland's richest mammoth site. In 1890 more than 100 bones, molar teeth and tusks of at least seven different mammoths were found, including a very young calf. All these findings were related to a peat horizon located at 3-4 meters below ground, the so-called "mammoth peat" (Furrer et al., 2007). A second peat horizon at a depth of 10-12.6 m was detected in a construction pit in 1987 and in three cores drilled in 1983 (KB 1-83, 2-83) and 1985 (KB 85) (Fig. 2-1) (Schlüchter, 1988b). Pollen analysis of this lower peat from KB 1-83 and KB 2-83 indicated a deposition during the Eemian interglacial (Welten, 1988). Moreover, Welten (1988) described a two meters thick paleosoil in the core KB 2-83, which was interpreted as being deposited probably during the penultimate glacial cycle.
In 2003 and 2004, new mammoth bones and even a well-preserved mammoth skeleton were found in two construction pits close to the 1890 mammoth pit (Furrer et al., 2007). The upper "mammoth peat" was again intensively investigated using many different methodological approaches. The upper part of the peat containing the mammoth skeleton and some peat and wood pieces were dated using radiocarbon dating and revealed an age of approximately 45 ^{14}C ka BP (Hajdas et al., 2007). The sediment above and below the mammoth peat was dated with luminescence dating to an age of ~40 ka and 80-70 ka, respectively (Preusser and Degering, 2007). Moreover, the analysis of pollen, wood and other plant material from the mammoth peat revealed a long phase of a former lake in the Wehntal, building swamps with different pollen associations partly dominated by *Picea* (spruce) in the upper part of the peat (Drescher-Schneider et al., 2007). This pollen association is an indicator for an improved climate with lower valley slopes partly covered by open mixed forest (Drescher-Schneider et al., 2007). In the lower part of the peat, the tree pollen concentration is very low, indicating unfavourable conditions for tree growth on the slopes of the Wehntal (Drescher-Schneider et al., 2007). Moreover, the research on

the mammoth peat from the 2003 mammoth site was complemented by the study of *Coleoptera* (beetles) by Coope (2007). An estimation of paleotemperatures based on *Coleoptera* assemblages in the peat showed similar climatic conditions as presently found near the northern limit of the boreal forest (Taiga) in Siberia (Coope, 2007). The different results of the studies on the 2003/04 sediment showed that the peat has developed during a more temperate period during the Würmian glacial cycle, starting after 80–70 ka in a shoaling lake and stopped around 40 ka by re-flooding (Furrer et al., 2007).

In October 2007, a 30 m deep core (NW07) was drilled close to the research site of 1985 and the pits in 2003/04 (Anselmetti et al., in press). Besides the two peat horizons other findings were made, which have not been detected in the previous drillings. One is the occurrence of deformation structures below the "Eemian peat" (around 140 ka), that suggested a temporary contact of the glacier with the lakebed. Another novelty was the detection of a sharp transition between the lake deposits and the "Eemian peat". This transition marked a lowering of the water level encompassing likely a hiatus (Anselmetti et al., in press). The age of the peat horizons and lake sediments using luminescence dating and pollen analysis agreed with the data from 2004. Moreover, the luminescence age of the bottom of the core is interesting for methodological purpose, since the method is still under development for ages around 200 ka. For the base of the 2007 core, the derived luminescence age is 190 ka (Anselmetti et al., in press).

3.2 Climatic aspects

In the course of the Quaternary, climate has changed several times from glacial to interglacial conditions and vice versa (Fig. 3-1) (Bassinot et al., 1994). Therefore, a more general view on the dominant atmospheric circulation patterns shows that both glacial and interglacial periods have their characteristic properties. Climate in general is mainly influenced by the interaction of three components: solar irradiation, atmospheric composition and terrestrial geography, whereas terrestrial geography did not change much during the Quaternary apart from growing and shrinking ice sheets (Harrison et al., 1992). Sub-parameters of these components are also the ones representing the most important boundary conditions for atmospheric circulation and climate on land. These are insolation, greenhouse gas concentration, ice sheets, sea-surface temperatures and sea-ice distribution (Harrison et al., 1992).
Today's and near past climate is well known and investigated through direct measurements or written records and the knowledge of the present atmospheric cir-

culation is essential for climate reconstructions. Nevertheless, as soon as climate has to be reconstructed in an indirect way using different climate proxies, there are several uncertainties coming across, increasing with the age of the time period being reconstructed. Additionally, past boundary conditions have rarely been the same as those today and hence, past climate cannot directly be inferred from the present conditions (Harrison et al., 1992). The investigation of paleoclimate is, however, an important topic in climate sciences. Therefore, several studies have been accomplished during the last decades about European and Swiss paleoclimate (e.g. Welten, 1988, Guiot et al., 1989; de Beaulieu et al., 2001; Martrat et al., 2004). Some important findings dealing with climatic conditions and fluctuations for the time period during MIS 6, MIS 5e and the transition between them are based on various glacial and pollen records, respectively.

The extent of Alpine glaciers during the MIS 6 has been discussed rather contro-

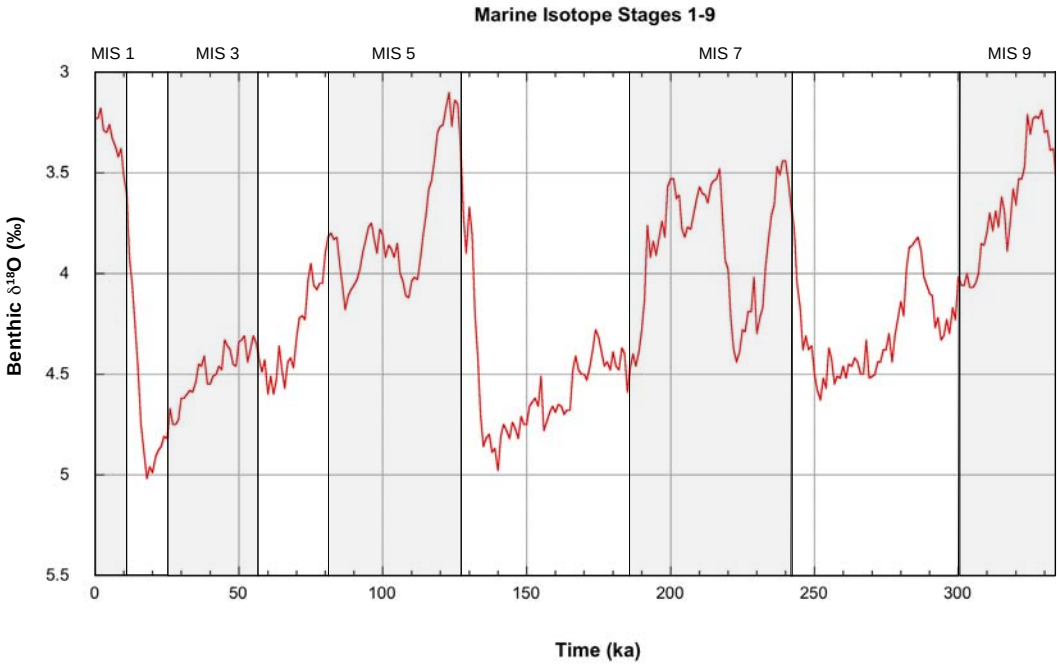

Figure 3-1: Marine Isotope stages 1-9 deduced from Benthic foraminifera $\delta^{18}O$ values. Low $\delta^{18}O$ values indicate a warmer climate and vice versa. Data source: Bassinot et al., 1994 (isotopic event stack) and Lisiecki and Raymo, 2005 (benthic δ18O data).

versially so far. While for this period, a major glaciation is assumed for the French (Buoncristiani and Campy, 2004) and Austrian (van Husen, 2004) Alps, the interpretation of Swiss records are different. Based on the Meikirch sequence in the Swiss Midlands, it has been deduced that the glaciation during MIS 6 must have been only of limited extent (Welten, 1988). However, a re-interpretation of the Meikirch pollen record by Preusser et al. (2005) using luminescence dating and results of penultimate glaciation erratic from the Jura Mountains by Graf et al. (2007) using exposure dating, gave evidence for a major glaciation of the Swiss Alps during MIS 6.

The transition from MIS 6 into MIS 5e has not yet been investigated extensively. Nevertheless, Sarnthein and Tiedemann (1990) discovered a general pattern for glacial terminations based on the findings from the last glacial-interglacial transition with its famous Younger Dryas cooling event and the analysis of benthic and planktonic foraminifera from a core offshore northwest of Africa. The analysis of the $\delta^{18}O$ values from this core revealed a fast cooling event after a first step of MIS 6 deglaciation at ~128.5 ka (Sarnthein and Tiedemann, 1990). Analogue to the Younger Dryas cooling event at the last glacial termination, benthic $\delta^{13}C$ minima revealed a breakdown of the North Atlantic Deep Water (NADW) formation immediately prior to the cold event at the penultimate glacial termination (Sarnthein and Tiedemann, 1990).
Furthermore, such a non-random nature for glacial-interglacial transitions and for the MIS 6 to 5e transition in particular, was detected by Seidenkrantz (1993) in two cores from Denmark and by Sànchez Goñi et al. (2000) in a marine core from the Iberian margin. Additionally, the benthic $\delta^{18}O$ values after Lisiecki and Raymo (2005) and the isotopic event stack after Bassinot et al. (1994) as well show indicators for such a cooling event at the MIS 6 to 5e transition (Fig. 3-2). For Central Europe and Switzerland, evidence for such a Younger Dryas-type cooling event during the transition from MIS 6 to 5e has not yet been found.

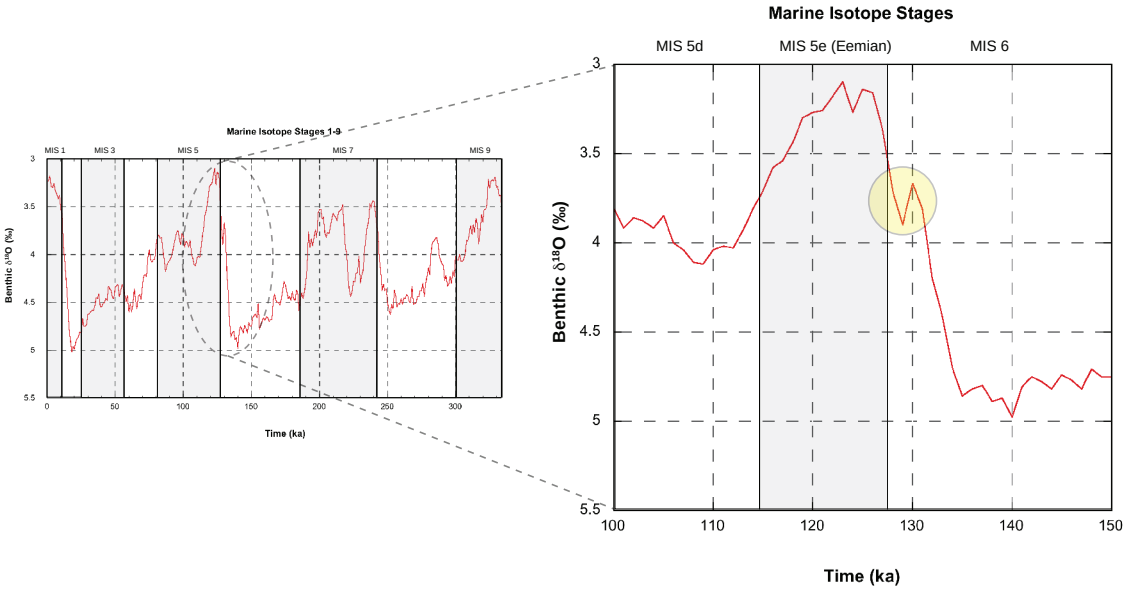

Figure 3-2: Detailed view on the transition from MIS 6 to 5e deduced from benthic $\delta^{18}O$. Low $\delta^{18}O$ values indicate a warmer climate and vice versa. Yellow circle indicates a possible „Younger Dryas“ cooling event afore the Eemian interglacial. Data source: Bassinot et al., 1994 (isotopic event stack) and Lisiecki and Raymo, 2005 (benthic $\delta^{18}O$ data).

4 Methodology

This chapter includes information about the different methods used to answer the given research questions. Due to the multidisciplinarity of the project, some data from investigations of other scientists within the research team are also used to answer the thesis' research question. For a better understanding of the results, these methods are described briefly in the paragraphs 4.1, 4.5 and 4.6. The chapter 4.7, describing luminescence dating, represents the main emphasis of this thesis and therefore is explained in more detail than the previous ones. A flow chart (Fig. 4-1), listing the proceeding of the laboratory work, all methods and the contributing scientists summarises this chapter.

4.1 Drilling

The 93.6 m long NW09 core was drilled by Stump ForaTec AG as the drilling operator. Rotary and percussion drilling techniques were used to recover the complete sequence of sedimentary basin fill including the top meters of the underlying molasse bedrock. The diameter of the sediment core decreases from 326 mm at the surface to 145 mm at 93.6 m depth. For further handling, the core was cut in 1 m pieces and stored in standard wood boxes. After the documentation, the remaining core material was transported and stored in the core repository of Schweizerische Landesgeologie at Hochdorf.

4.2 Sediment description and sampling

The upper third of the core pieces was cut off using a guitar string and then removed. For continuous sampling, one half of a plastic pipe, the so-called u-channel, with a diameter of approximately 4 cm was hammered into the lower two-third of the core. To remove the u-channel, the core was cut again just below the plastic pipe. The u-channel then was closed with a lid and sealed with tape to avoid water and sediment loss. Parts of the surrounding sediment of the cut slice were used for further sampling discussed later in this chapter (Fig. 4-1). In general, two samples were taken from each core section, one at 30 cm and one at 70 cm starting from top of the core piece. Each sample was sub-sampled into three cubes of 3-5 cm^3 for the purpose of grain-size, geochemistry and pollen analysis. In sections with prominent sediment colour or grain-size changes, the number of samples was increased.

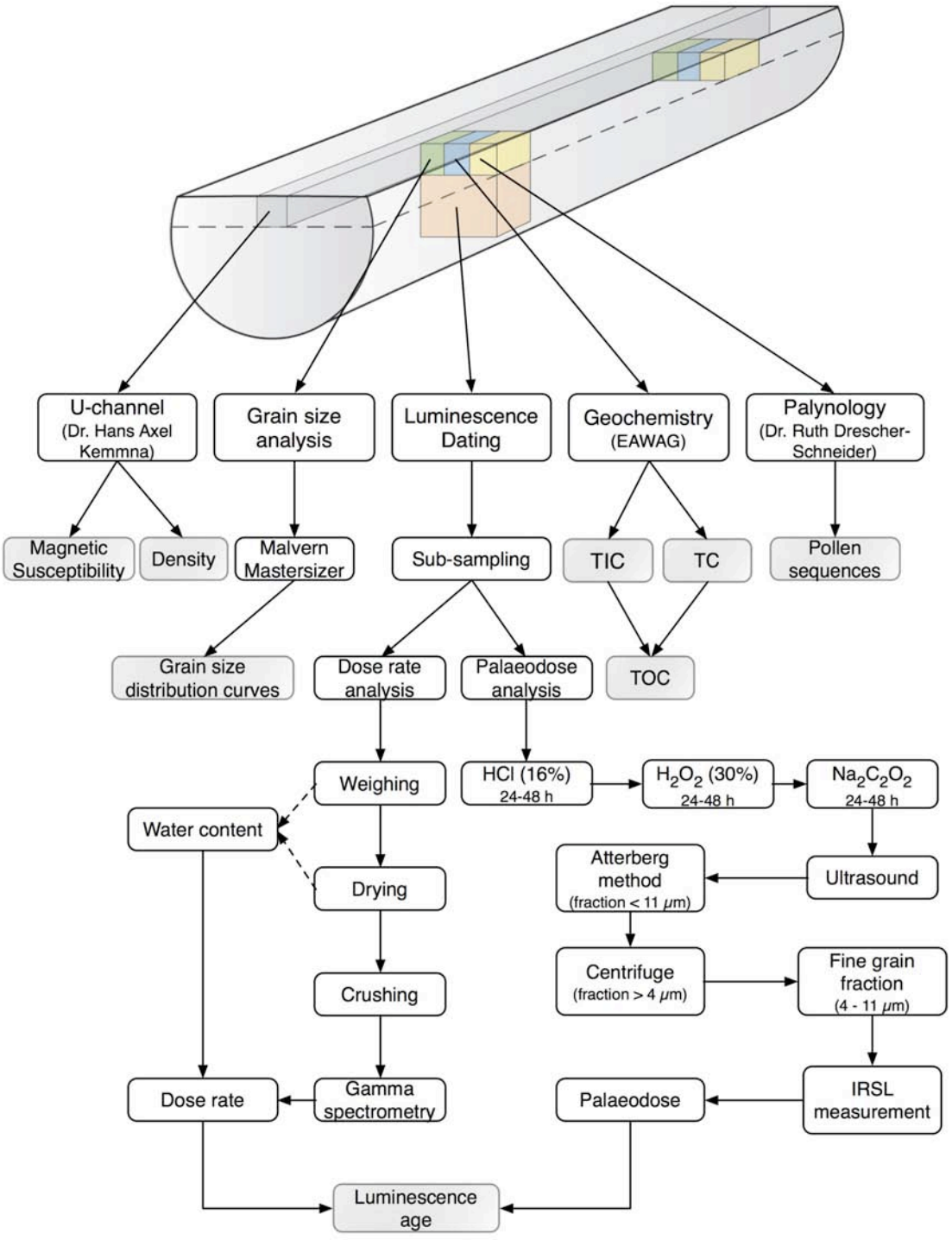

Figure 4-1: Flow chart of the methods used. Gray boxes show research results.

The sampling for luminescence dating was conducted after documentation of the core and is explained separately (in chapter 4.7.3) due to its particular proceeding. After sampling, the shear strength of the sediment was measured using a torsional vane shear tester.

For the documentation of the core, high-resolution photographs were taken every 20 cm and sketches of the opened cores were drawn. These sketches include sediment colour, lamination, grain-size, conspicuous structural patterns and sub-sampling positions.

4.3 Grain-size analysis

Grain-size analysis of the whole NW09 core was carried out using the Mastersizer 2000 from Malvern Instruments. The Mastersizer measures grain-sizes from 0.2 up to 2000 µm using the laser diffraction technique (Malvern Instruments, 2010). For the measurement, a knife point of sample material was dispersed in deionised water until an obscuration value of 10-20% was reached. A stirrer and an ultrasound unit were used to dissolve particle agglomerates and destroy air-bubbles possibly skewing the data. The stirrer was adjusted at a medium value of 1450 rpm and the ultrasound at an intensity of 50–70%. When the required obscuration value was reached, the sample was directly channelled into the measuring chamber, where a laser beam then is scattered by the particles in suspension. The resulting scattering angle is closely dependent on the size of the particle (Malvern Instruments, 2010). After each measurement cycle, the system was cleaned three times to maintain clean conditions. The measurement results are automatically processed to a data-sheet including particle size distribution plots and detailed numerical results. For the presentation of the measurement results, the median grain-size (in µm) was selected, in order to provide an appropriate coverage of the marginal values measured.

4.4 Total inorganic and total carbon content

The carbon content of a sediment sample can be derived extracting its CO_2 concentration by either burning (total carbon) or acidification (inorganic carbon) (Herrmann and Knake, 1973). For the measurement, the samples were freeze-dried for at least 24 hours. To measure the total carbon content (TC), the CO_2 is extracted from the sediment, packed in an aluminium capsule and burning it at 950°C. To determine the total inorganic carbon content (TIC), ca. 20 mg of sample material was acidified with perchloric acid (32%). Thereby, the CO_3^{2-} of the sample reacts with the perchloric acid and CO_2 is released. The CO_2 is channelled to the measurement cell of the coulometer (Coulometer CO_2 CM 5011, from UIC Inc. Coulometrics). This measurement cell consists of a cathode and an anode. The CO_2 induced changes the transmissibility and the electricity current of the cathode solution. To recover the initial transmissibility of the cathode solution, the coulometer increases the elec-

tricity current through the measurement cell. Based on the amount of additional electricity, the Win-Carb software calculates the original C content (in wt-%) of the sample. At the beginning, after six to eight measurements and at the end of each cycle, a standard $CaCO_3$ sample (with 12 wt-% C) was measured to control measurement uncertainty. The amount of total organic carbon (TOC) was calculated using the difference between TC and TIC.

4.5 Density and magnetic susceptibility

The u-channels were tested for density and magnetic susceptibility using a multisensor core logger from Geotek Ltd. These indicators provide information concerning lithology changes (density) and provenance analysis (magnetic susceptibility). The density was calculated using the attenuation of gamma rays, which were shot through the u-channel with an interval of 1 cm and a duration of 5 seconds whereas the magnetic susceptibility was measured every 4 cm but for a duration of 10 seconds.

4.6 Palynological analysis

Palynological investigations were done in the laboratories of the Botanical Institute at the University of Graz by Dr. Ruth Drescher-Schneider. In total, 372 samples for palynological analysis were taken from the NW09 core at about 5-50 cm intervals. From this set, 39 samples are analysed so far. For the preparation, the samples were treated with hydrofluoric acid (37%) to remove inorganic material. Partially, a second treatment with hydrofluoric acid (74%) and sometimes even a separation with heavy liquid ($ZnCl_2$) was necessary due to insoluble mineral fragments. For each sample, 500 pollen grains were counted and analysed. As in cold period deposits the pollen concentration was very low, the analysis was limited to an area of 24×32 mm. The given pollen sum includes trees, shrubs and terrestrial herbs (Drescher-Schneider, unpublished data).

4.7 Luminescence dating

The dating of the samples from NW09 was conducted in the luminescence laboratory of the Institute of Geological Sciences at the University of Bern using infrared stimulated luminescence (IRSL). Due to the importance of reliable sediment ages for significant results, the IRSL method was chosen as it has already been used suc-

cessfully in former projects in this area (Preusser and Degering, 2007; Furrer et al., 2007). Luminescence dating is a complex topic, but the basic ideas of the phenomenon for dating Quaternary sediments are quite simple (Duller, 2004). The following chapter tries to give an understanding of the essential processes of luminescence dating.

4.7.1 Introduction

The phenomenon of luminescence, which describes the release of energy in the form of light, has been known and observed for a long time in many different ways (Duller, 2004). Among these phenomena, bioluminescence is the most common and was mentioned in reference to fireflies in early Chinese literature 3,000 years ago (Aitken, 1998). However, first scientific investigations were not conducted until the mid-seventeenth century, when Boyle (1664, in Aitken, 1998) did a few first experiments with a kind of diamond, emitting cold light (Lian and Roberts, 2006; Aitken, 1998). Luminescence as a dating technique was discovered after the invention of the photomultiplier in the 1920s (Aitken, 1998).

The method of luminescence dating is based on the principle that mineral grains store a certain amount of energy over time. From this energy stored in the crystal lattice of the minerals, the time since crystallisation, last exposure to sunlight or to heat can be derived (Lian and Roberts, 2006). As this method uses minerals with a thermally and optically sensitive luminescence signal such as quartz and feldspars (Preusser et al., 2008), the signal can be erased by heating or illumination (Aitken, 1998). In the context of dating lake sediments the resulting date refers to the last deposition of the sediment at which the mineral grains were exposed to daylight (Stokes, 1999). This daylight exposure is known as bleaching and erases the latent luminescence signal. When the mineral grains are covered with sediment and the daylight is shielded, the latent luminescence signal accumulates again (Preusser et al., 2008) (Fig. 4-2). This accumulation results from a weak flux of ionizing radiation provided by the decay of radioactive elements within the minerals and the surrounding sediment, as well as by cosmic rays (Lian and Roberts, 2006; Aitken, 1998). Thus, the intensity of a luminescence signal is depending on the amount of energy the mineral has absorbed since the last bleaching event and is referred to as Paleodose, measured in the unit of grays (1 Gy = 1 J kg^{-1}) (Duller, 2004; Stokes, 1999). If now the rate at which the sample was exposed to radiation over time, the so-called dose rate (in Gy ka^{-1}), is known and if this rate was constant over time, then the luminescence age can be derived using equation [1] (Duller, 2004; Aitken, 1998):

$$\text{Luminescence age (a)} = \frac{\text{Paleodose (Gy)}}{\text{Dose rate (Gy ka}^{-1})} \quad [1]$$

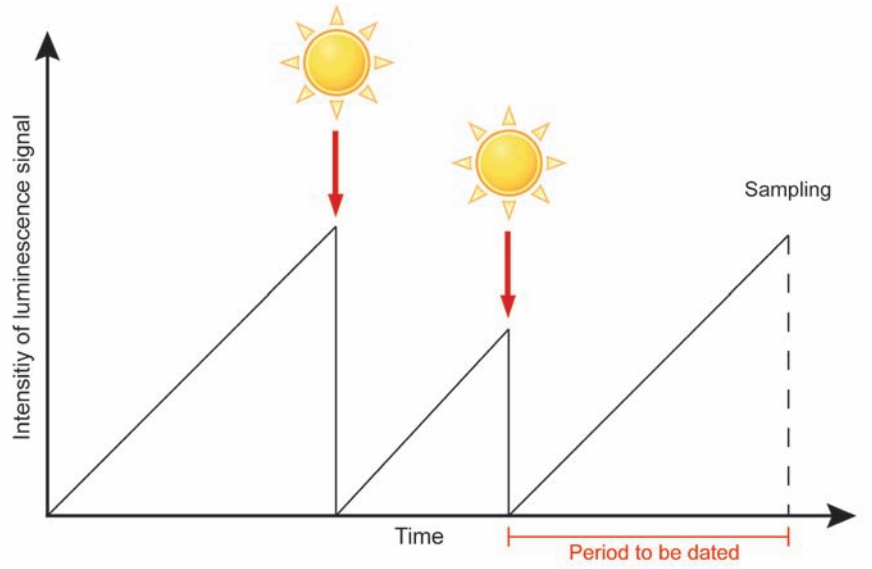

Figure 4-2: Basic principle of luminescence dating: accumulation of the signal over time when the material is sealed from daylight and not exposed to heat, followed by a zeroing of the signal during daylight exposure or heating. The luminescence age reflects the last zeroing of the signal. Redrawn after Preusser et al. (2008).

For a better understanding of the physical mechanism behind the occurrence of luminescence, the energy-level representation (Fig. 4-3) is used as a basis of explanation. Ionizing radiation originating from the surrounding sediment and cosmic rays excites the atoms within the crystal lattice, leading to an activation of electrons reaching a higher energy state (Aitken, 1998; Duller, 2004; Preusser et al., 2008). Most of the activated electrons leave their higher energy state immediately and recombine with a hole in the valence band. A small part of the excited electrons, however, are trapped in energy states below the conduction band, the so-called electron traps (Krbetschek et al., 1997; Aitken, 1998; Preusser et al., 2008). These electron traps represent defects in the crystal lattice, which occur in naturally grown crystals (Aitken, 1998). Due to this effect, a charge deficit in form of holes is generated in the valence band. These holes act as recombination centres being filled by electrons from localised levels above the valence band (Preusser et al., 2008). If radiation continues, more and more electrons are trapped over time, increasing the latent luminescence signal. Due to a bounded number of electron traps, the latent signal will be saturated at a certain point. This condition is referred to as saturation (Lian and Roberts, 2006; Preusser et al., 2008).

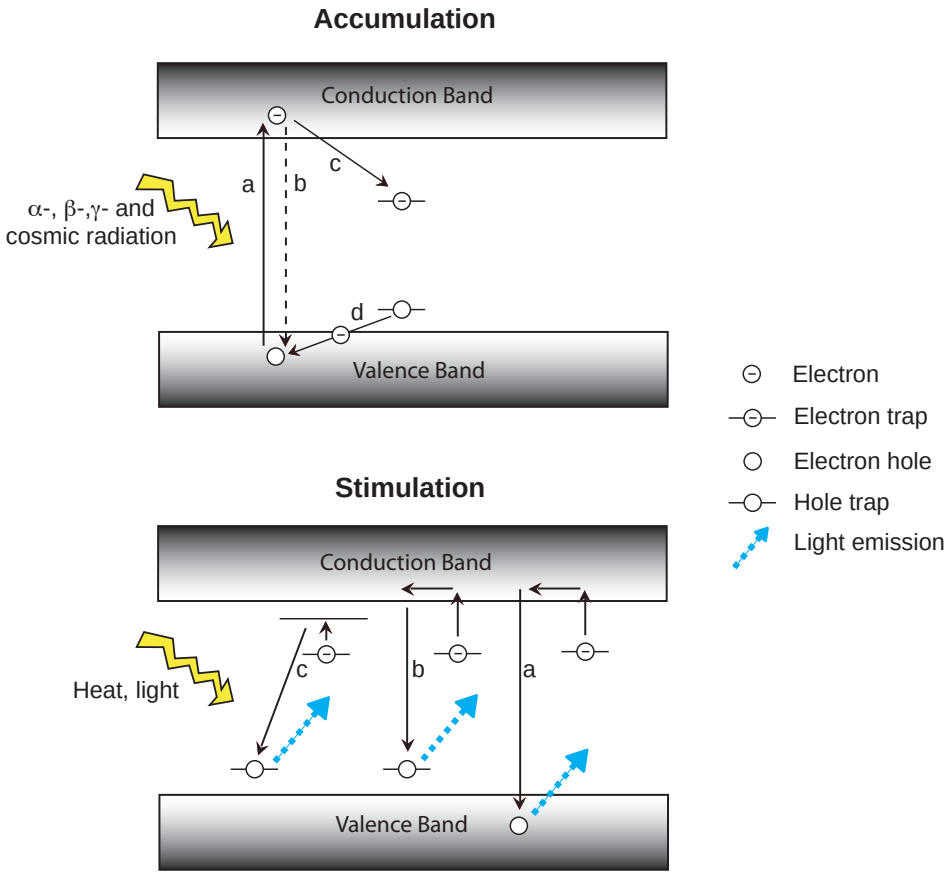

Figure 4-3: Simplified energy level model. Schematic illustration of the processes during accumulation (left) and stimulation (right). Redrawn after Preusser et al. (2008).

Accumulation:
- a: Electron is excited by ionising radiation and has sufficient energy to reach the conduction band, leaving a hole in the valence band.
- b: Most of the electrons recombine immediately with a hole in the valence band.
- c: A few excited electrons reach localised energy states below the conduction band and are trapped in electron traps.
- d: The hole in the valence band may be filled by electrons from hole traps (localised levels above the valence band). This is referred to as the hole transfer from the valence band to the localised level.

Stimulation:
- a: Electron is excited by light or heat and leaves the electron trap through a recombination with a hole in the valence band. The loss of energy in all three cases may be released in the form of light (=luminescence).
- b: Recombination of the electrons with localised hole traps above the valence band via the conduction band.
- c: Recombination of the electrons with localised hole traps after a transfer to an unstable level below the conduction band. (Preusser et al., 2008)

When a mineral is exposed to a certain dose of stimulation energy, the electrons are released from the traps (Duller, 2004; Preusser et al., 2008). Such stimulation energies can result from heating or irradiating the mineral, which leads to lattice vibrations (Aitken, 1998). Not all electron traps have the same energetic depth and therefore the amount and type of energy needed to release an electron varies. The deeper a trap is the higher is the required stimulation energy (Aitken, 1998; Preusser et al.,

2008). Once an electron has been emitted from a trap, it diffuses around the crystal until a recombination centre is found. During this recombination process, some of the energy stored is released from the electron in the form of light. This is the light referred to as luminescence and being measured by the luminescence reader (Aitken, 1998; Preusser et al., 2008).
The amount of recombining electrons is proportional to the electrons trapped during accumulation and the intensity of light emitted during the stimulation process (Aitken, 1998; Preusser et al., 2008). A more detailed review of the general concept of luminescence dating is given in Aitken (1998), Duller (2004), Lian and Roberts (2006) and Preusser et al. (2008).

4.7.2 Infrared stimulated luminescence

Luminescence dating includes different methods working all with the same physical principle of light emission during recombination processes as mentioned above. The two main approaches are luminescence dating using thermal and optical stimulation. Thermoluminescence (TL) comprises the stimulation by heating the mineral up to a certain temperature leading to electron recombination and hence to light emission (Preusser et al., 2008). Luminescence dating applying optical stimulation includes mainly two different stimulation sources, the stimulation by visible light (optically stimulated luminescence, OSL) and by infrared light (infrared stimulated luminescence, IRSL). The major advantage of optical methods over thermoluminescence is that only the light-sensitive part of the luminescence signal is stimulated and thus the signal is much faster bleached during deposition in comparison to heat sensitive parts (Preusser et al., 2008). The IRSL signal of feldspars is used for sediment dating purpose since the work of Hütt et al. (1988). For the polymineral fine-grained sediment samples from the NW09 core, the IRSL method was adopted. The main advantage of IRSL over OSL is that a much wider wavelength range is available for the detection of the luminescence signal. Further, the IRSL signal is more effectively bleached at deposition than the luminescence signal stimulated by visible light (Aitken, 1998).

4.7.3 Paleodose determination and SAR-protocol

For the calculation of the luminescence age, the determination of the paleodose is a prerequisite. To obtain the paleodose, a dose function is calculated which allows to deduce the dose accumulated over time from the luminescence signal of a mineral grain. The relation between paleodose and luminescence intensity is quite simple:

the higher the paleodose, the higher the luminescence intensity. Furthermore, the number of defects in the crystal lattice of a mineral is responsible for its luminescence intensity (Aitken, 1998). The number of these defects, however, is dependent on the conditions during crystallisation of the mineral, its geological history and the amount of surrounding radioactive radiation (Bøtter-Jensen et al., 2003; Atiken, 1998). Therefore, the luminescence intensity of crystals from the same mineral can vary to a great extent (Lian and Roberts, 2006). Hence, the luminescence intensity is not directly reflecting the paleodose. In fact, the paleodose has to be estimated by comparing the natural signal with laboratory-induced signals. With this approach, the dose of radiation required to obtain a luminescence signal equal to the natural signal can be derived (Lian and Roberts, 2006). As this derived radiation dose is a laboratory-induced dose, which is equivalent to the natural paleodose, it is referred to as equivalent dose (D_e) (Lian and Roberts, 2006).

The methodological approach to achieve the dose function for this study is the single-aliquot regenerative-dose (SAR) protocol, mainly developed by Murray and Roberts (1998) and Murray and Wintle (2000, 2003). Although the SAR protocol was developed for OSL measurements of quartz minerals, Wallinga et al. (2000) proved its application for IRSL dating of feldspars. In comparison to the additive method, where an artificial signal is added to the natural signal, the regenerative method first measures (and at the same time removes) the natural signal before the laboratory signal is induced. Using the regenerative dose method, the equivalent dose is obtained by direct comparison of the natural luminescence signal with a series of laboratory irradiations (Fig. 4-4) (Aitken, 1998).

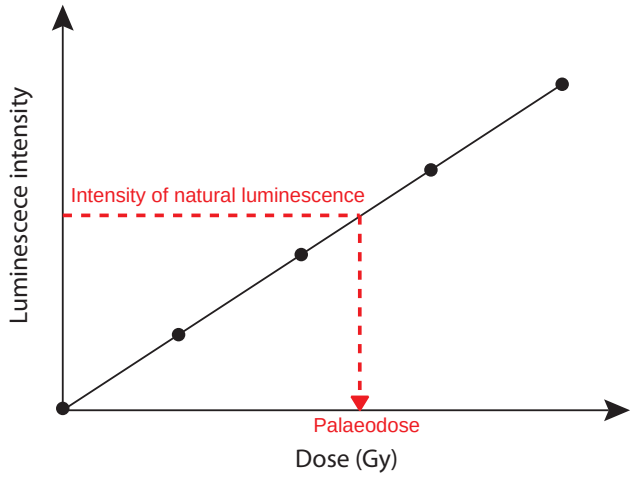

Figure 4-4: Dose response curve of the regenerative method. After the measurement of the natural signal, different laboratory doses are induced to the aliquots and the luminescence responses to these doses are used to construct a growth curve. The paleodose can then be evaluated by a projection of the natural signal on the growth curve. Redrawn after Preusser et al. (2008).

A major advantage of the regenerative method is that only interpolation and no extrapolation is involved, whereby uncertainties due to nonlinearity are reduced (Aitken, 1998; Preusser et al., 2008). As the SAR protocol only uses one single sub-sample for each measurement, which is referred to as aliquot, a change in luminescence sensitivity occurs due to repeated bleaching of the same mineral grains. To monitor these sensitivity changes, a test dose is implemented in the measurement protocol. This test dose is administered on the same aliquot immediately after the signal from the natural dose and every regenerative dose has been measured (Murray and Wintle, 2003; Lian and Roberts, 2006) (Fig. 4-5).

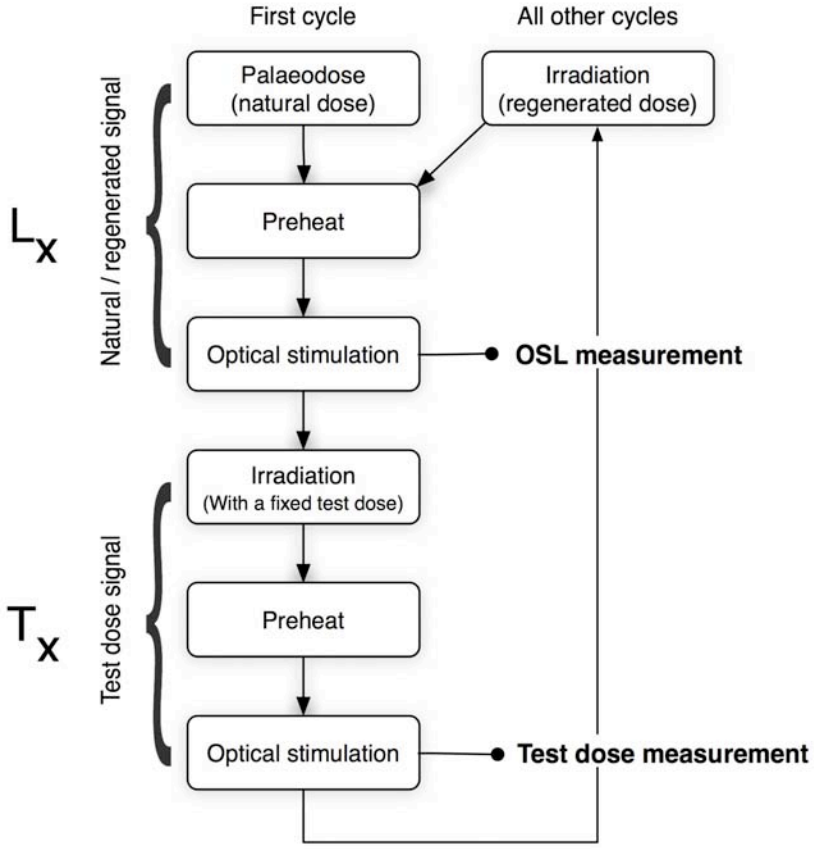

Figure 4-5: Schematic illustration of the standard single-aliquot-regenerative-dose (SAR) protocol of Murray and Wintle (2000, 2003). LX is the natural (first cycle) or regenerated (all other cycle) signal measured and TX is the signal of the test dose measured after each natural or regenerated signal. Redrawn after Preusser et al. (2008).

The test dose remains constant during the whole protocol and is in the range of 10-20% of the natural dose as suggested by Murray and Wintle (2000). The luminescence signal of the test dose (T_x) is used to normalise the regenerated signals (L_x). Therefore, the ratio of L_x and T_x (L_x/T_x), representing the sensitivity-corrected luminescence signal, is calculated to construct a dose response curve (Fig. 4-6) (Preusser

et al., 2008). After the measurement of at least three different regenerative doses, the natural dose and the zero dose, the curve can be fitted to these dose points. To improve the mathematical fitting of the dose response curve, the flexibility of the SAR protocol allows running further cycles with other regenerative doses (Preusser et al., 2008).

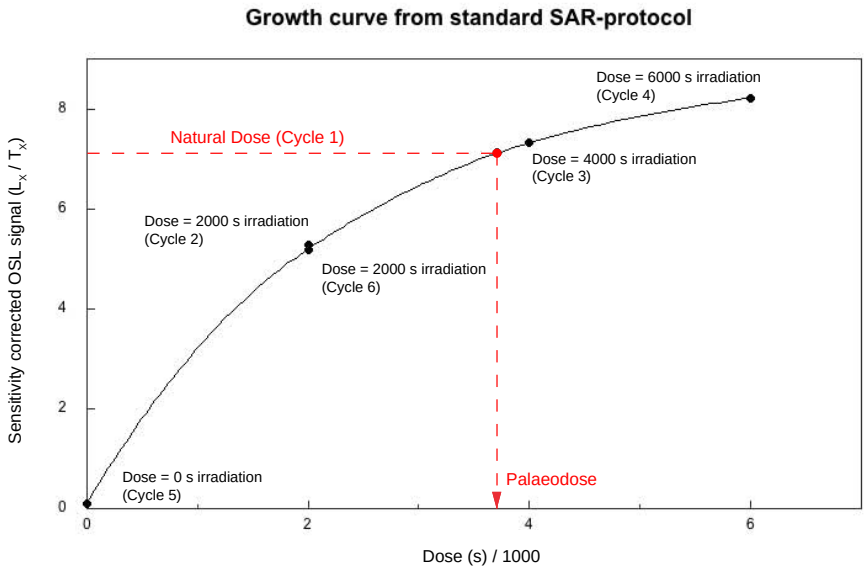

Figure 4-6: Growth curve of the standard SAR-protocol applied to NW09 samples. The signals of the natural and regenerated measurements are divided by the signal of the test dose to apply a sensitivity correction. To control the sensitivity correction, the same regenerated dose is measured in the measurement cycles two and six. The ratio of these two measurements is referred to as recycling ratio and should not exceed a value of 0.1 (Preusser et al., 2008).

4.7.4 Sampling

Sampling for the luminescence sub-samples was done after the documentation of the sediment (chapter 4.2). Cubes of sediment of approximately 10-15 cm^3 were cut out of the sediment core and immediately packed in labelled opaque plastic bags. Samples for the paleodose determination must not be exposed to light during the sampling procedure, as already a short time of light exposition can lead to a bleaching of the luminescence signal and hence to an age underestimation. The layer from which the sediment is taken should preferably be homogeneous and with a thickness of approximately 30-50 cm in order to ensure a uniform radiation field (Aitken, 1998; Preusser et al., 2008). A total of 24 samples were taken from the NW09 core. The samples were labelled as “NWE”, going from NWE1 at the bottom to NWE24 at the top of the core (Table 4-1).

Sample	Depth (m)	Sample	Depth (m)
NWE1	91.45	NWE13	35.23
NWE2	86.45	NWE14	32.46
NWE3	80.6	NWE15	29.25
NWE4	77.8	NWE16	24.27
NWE5	73.85	NWE17	19.55
NWE6	69.41	NWE18	16.2
NWE7	60.36	NWE19	14.89
NWE8	53.71	NWE20	12.49
NWE9	48.53	NWE21	11.55
NWE10	45.31	NWE22	10.57
NWE11	40.3	NWE23	5.65
NWE12	38.5	NWE24	3.5

Table 4-1: Sample name and sample depth of all IRSL samples taken from the NW09 core.

4.7.5 Sample preparation

To avoid unwanted stimulation or loss of luminescence, the preparation and measurement steps for the determination of the paleodose were done in the low intensity red-light laboratory of the Institute of Geological Sciences at the University of Bern. The sample preparation is conducted in order to separate the samples into portions or aliquots of different mineral grains of a given size range and mineral composition. These aliquots are then placed on small metal discs with a diameter of 10 mm and a thickness of 0.5 mm to carry out the luminescence measurement. Only the inner part of the sample was taken for paleodose measurements to assure that the sediment was not exposed to light during the drilling and sampling process. Therefore, the outer 4-5 cm of the sample cube were cut off. The sediment removed was used for the dose rate determination, as there is no need for a shielding from light for this purpose. These sub-samples were weighed and dried in an oven at 60°C for approximately 48 hours. In this working step, the current water content of the sediment was deduced by means of the weight difference before and after drying, as the water content is used for the determination of the dose rate (*chapter 4.7.8*). After drying and weighing, the sub-sample material was crushed using a jaw breaker to loosen the sediment, which stuck together due to its high clay and silt content. The crushed dose rate samples were filled into special boxes for the following gamma spectrometry described in chapter 4.7.8.

The preparation for the polymineral fine-grain IRSL measurement was carried out according to the instructions given in Preusser et al. (2008). To remove all carbonates, the samples were treated with 16% hydrochloric acid (HCl). Organic material was

removed using 30% hydrogen peroxide (H_2O_2). The treatment with diluted sodium oxalate ($Na_2C_20_4$) acting as a dispersion solution released the mineral grains from clay pads. An ultrasound irradiation of 3-4 minutes completed the dispersion with sodium oxalate. The treatments with HCl, H_2O_2 and sodium oxalate took all between 24 and 48 hours, depending on the carbonate, organic material and clay content, respectively. Rinsing the samples three times with deionised water followed every preparation step. Fine-grain measurements include a grain-size from 4-11 µm. For an isolation of this fraction, the elutriation method after Atterberg, based on Stokes' Law (Tucker, 1996), was applied. The elutriation process was repeated several times until the obscurity of the water after settling was very low being an indicator that all mineral grains with a grain-size >11 µm are eliminated. After each elutriation cycle, the remaining sediment was centrifuged to remove the grain-size <4 µm and thus the grain-size between 4 and 11 µm needed for the fine grain measurement remained. The last preparation step after drying the sediment in an oven at 60°C was the placing of the aliquots on the small metal discs. Therefore, the sub-sample was brought in suspension with acetone (C_3H_6O) and filled in a glass pipe from where it settled down on the disc. These aliquots are then placed on the sample carousel of the luminescence reader for the IRSL measurements.

4.7.6 Testing procedure

Prior to the actual paleodose measurement, a number of tests were carried out to ensure the quality and reliability of the results. As the minerals from different geological settings differ in their luminescence properties, it is necessary to test for dose recovery, preheat temperature, thermal transfer and anomalous fading (Preusser et al., 2008). By reasons of comparability and regularity, different aliquots from the same sample were used throughout the test period.

A first test concerned the retrieval of the dose induced in the laboratory by the measurement process. During the so-called *dose recovery test*, the natural dose was erased and a known laboratory dose was administered to the sample. The laboratory dose resulted from an irradiation by a $^{90}Sr/^{90}Y$-β-source over 4000 seconds. This dose was then treated as the natural signal in the standard SAR-protocol (Preusser et al., 2008). In the optimal case the measured dose should be equal to the given dose. If the deviation is too large, changes in the measurement protocol have to be applied.

The choice of an appropriate preheat temperature can pose one possible source of

error. Preheating is implemented prior to the measurement step in the SAR protocol (see Figure 4-5) and leads to the removal of unstable luminescence from shallow traps (Aitken, 1998). To evaluate the ideal preheat temperature, the SAR-protocol was carried out using preheat temperatures at 230°C, 250°C, 270°C and 290°C. This process is known as *preheat test*. At a certain temperature, the unstable signal is removed and the paleodose should remain stable (Figure 4-7).

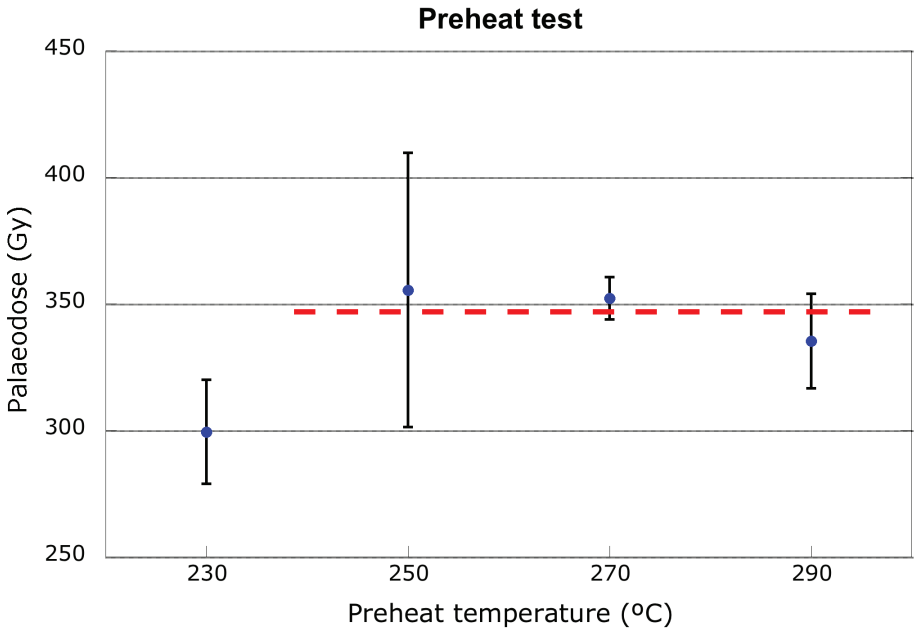

Figure 4-7: Results of a preheat test of the sample NWE18. The preheat test is conducted to determine the ideal preheat temperature. The red dotted line reflects the so-called preheat plateau, representing the threshold value for a stable signal. In this example, a preheat temperature of 270°C was chosen.

These stable values represent the so-called preheat plateau (Murray and Wintle, 2000) and the ideal preheat temperature is situated in the range of this preheat plateau. For the NW09 core, dose recovery and preheat test were merged to the same SAR measurement sequence (see appendix).

If the preheat temperature is too high, stable electron traps may be transferred to unstable traps leading to an overestimation of the paleodose (Preusser et al., 2008). This effect is referred to as thermal transfer and can be identified by erasing the latent luminescence signal and then measuring the paleodose. The resulting paleodose should not be significantly higher than 0 Gy (Preusser et al., 2008). This test is known as *thermal transfer test*.

The last test addresses the loss of luminescence signal with time. This occurrence of anomalous fading leads to an underestimation of the paleodose due to the instability of some electrons over time (Duller, 2004). Most of the electrons captured in a particular trap are stable. But some of them do not have the same lifetime and therefore are evicted over time without any additional stimulation energy. This leads to the

underestimation of the paleodose since the laboratory-induced signal still contains a part of the unstable charge, even after preheating (Preusser et al., 2008). To derive the loss of the signal with time, the *fading test* was applied. Therefore, a regenerative dose, resulting from a β-source irradiation of 800 seconds, was induced to the same sample several times, but with different time intervals between preheating and measurement. For the NW09 core, time intervals of 400, 580, 1000, 2200, 4000, 7600, 400 and 580 seconds were applied. If this test reveals a significant fading rate, the so-called g-value, the derived luminescence ages are corrected after the dose rate correction equation of Lamothe et al. (2003).

To control the reliability and quality of the SAR cycles during the IRSL measurements, two internal tests were carried out. The *recuperation-test* was used to check, whether preheating the sample generated an unwanted signal (recuperation). To control this, the ratio between the signal from an aliquot given zero regenerative dose and the test dose (L_0/T_0) should be close to zero and after Murray and Wintle (2000) not exceed 5% of the sensitivity-corrected natural dose (L_N/T_N) (Preusser et al., 2008). The *recycling ratio test* controls whether the sensitivity correction applied was appropriate. Therefore, a dose identical to the first regenerated dose was measured at the end of the SAR cycle. If the ratio between these two measurements (recycling ratio) was ≤10%, the sensitivity correction was appropriate (Preusser et al., 2008).

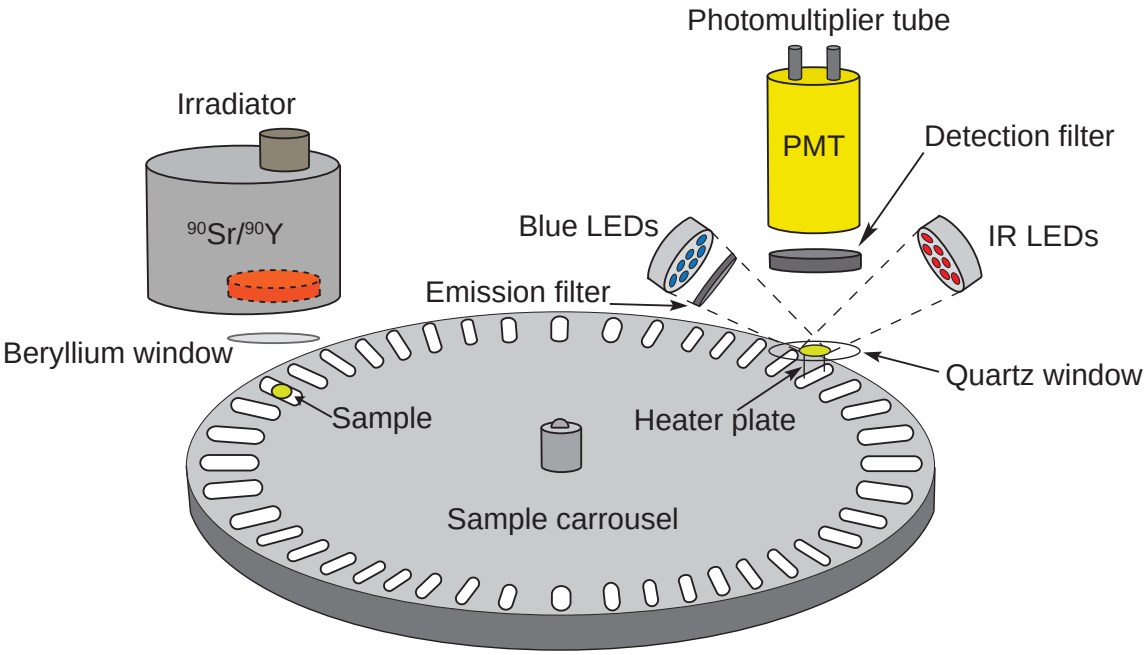

Figure 4-8: Schematic sketch showing the basic features of the Risø TL/OSL reader. Further technical information in Bøtter-Jensen et al. (2003). Redrawn after Risø (2010).

4.7.7 IRSL measurement

Paleodose measurements are conducted on the most commonly used luminescence reading device manufactured by the Risø National Laboratory, Denmark. As the paleodose determination consists of different consecutive steps, the luminescence reader has to combine all these different devices in one single apparatus (Fig. 4-8). The three main steps are irradiation, pre-heating and measurement of luminescence. During these steps, the samples were placed on a sample carousel in the measurement chamber. The sample carousel automatically positioned the aliquots stepwise below the irradiation unit and the stimulation and detection unit. As already mentioned, a $^{90}Sr/^{90}Y$ β-source was used for irradiation purpose to induce a latent luminescence signal to the mineral grains. This β-source accumulates a luminescence signal with a rate of 0.1066 Gy s^{-1} to the aliquots. The preheating was done using a sample-heating device. For measurement purpose, an infrared LED stimulation source and a luminescence detection unit including a photomultiplier tube and optical filters are integrated. The LED light serves as stimulation energy leading to a de-trapping of electrons and thereby to luminescence emitting recombination (Preusser et al., 2008).
The measurement protocol containing all measurement parameters was written as a sequence in the Risø Sequence Editor software, version 3.2.1, 2007. Moreover, the Sequence Editor is the interface between measurement protocol and the luminescence reader. The analysis of the measurement results was carried out on the Risø Luminescence Analyst software, version 3.24, 2007.

4.7.8 Dose rate determination

Referring to equation [1], the divisor, representing the dose rate, of the age equation is needed to calculate the luminescence age. The dose rate is the energy (J) per mass (in kg) and time (in ka), impacting on the sample in the form of naturally occurring ionising radiation (Aitken, 1998). This ionizing radiation is composed of the decay of radioactive elements within the minerals (internal dose rate) and the surrounding sediment (external dose rate), as well as of cosmic rays (cosmic dose rate). The naturally occurring ionizing radiation in the sediment appears in the form of α-, β- and γ-radiation (Aitken, 1998; Preusser et al., 2008). All of these radiation types have different penetrating powers, but as for the NW09 core only fine grain IRSL measurements were carried out with a grain-size range from 4-11 µm, they all penetrate the grains completely (Aitken, 1998). Most of the dose rate radiation originates from naturally occurring radionuclides in the sediment, whereas radiation from ionising cosmic rays contributes only to a minor amount to the dose rate and is dependent on

the latitude and burial depth of the sediment (Aitken, 1998).

The dose rate is determined by measuring the radionuclide activity followed by the conversion with a conversion factor, based on nuclear data tables (cf. Adamiec and Aitken, 1998). Here, high-resolution gamma spectrometry was used to derive the radionuclide activity. This radionuclide activity originates from the decay of the unstable radionuclide ^{40}K and from the ^{238}U, ^{235}U and ^{232}Th decay series (Fig. 4-9). Such a nuclide aims for a stable state and therefore may need to decay several times until the stable state is reached (Geyh, 2005). The gamma spectrometry measurements were conducted at the Chemical Institute of the University of Bern by PD Dr. Soenke Szidat. To simplify the calculation, the following general assumptions concerning the material and the radionuclide concentrations are made: a homogeneous distribution of the sources of ionising radiation, an indefinite expansion of the investigated system and constant radionuclide concentrations over time (Preusser et al., 2008). Despite these assumptions, there are a couple of potential nonconformities, which have to be taken into account. One is the water content of the sediment. The water in the sediment pores absorbs much more radiation than air does. Therefore, the dose rate for dry sediment is higher than for the same sediment in wet conditions (Aitken, 1998).

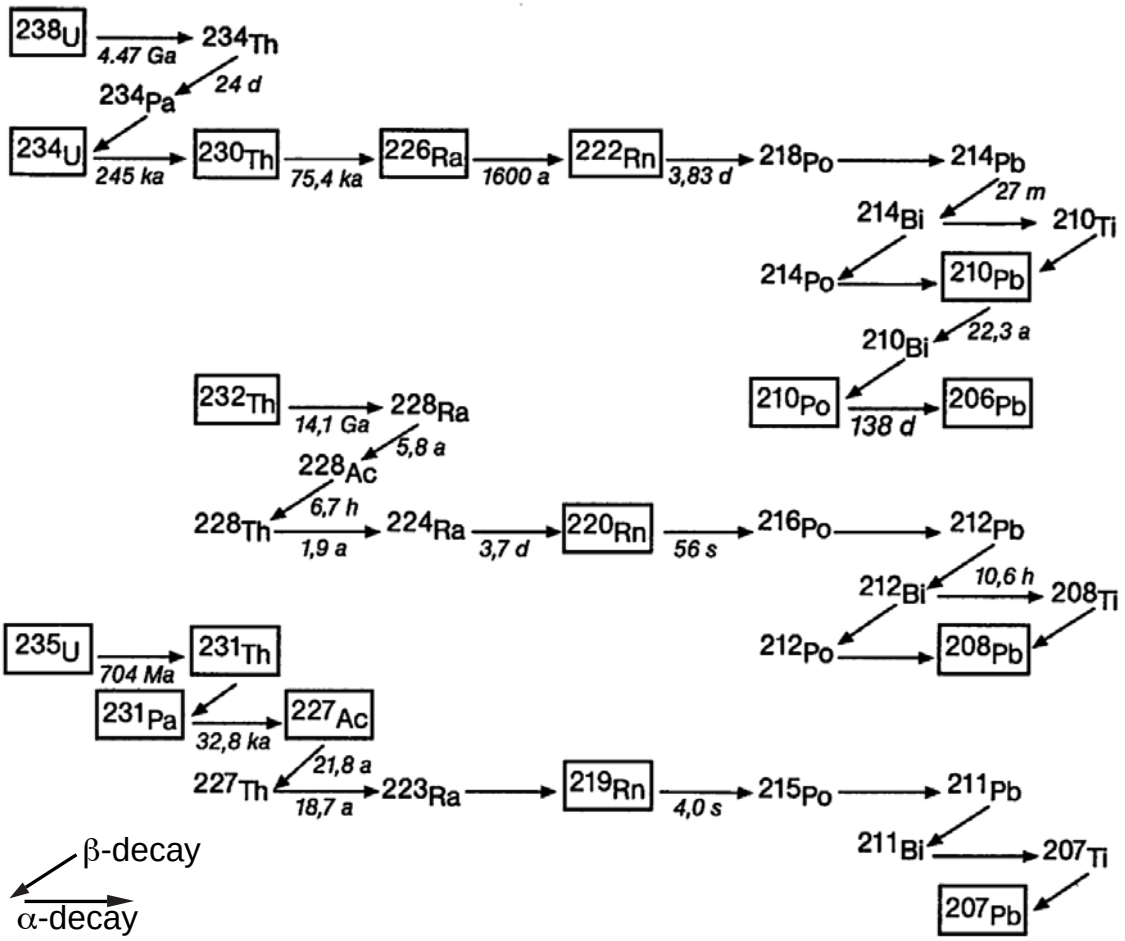

Figure 4-9: Illustration of the ^{235}U, ^{238}U and ^{232}Th decay series with the corresponding half-life times. Source: Geyh (2005).

A second problem is the occurrence of radioactive disequilibria. In a closed system, the decay series of thorium and uranium are in equilibrium. This means that the rate of decay of each daughter isotope is equal to the rate of decay of its parent (Aitken, 1998). In an open system, due to removal or addition of daughter isotopes, some of the daughter decay rates are no longer equal to their parent's activities. This state is referred to as radioactive disequilibrium (Aitken, 1998). To check the presence of this equilibrium, high-resolution gamma spectrometry is a suitable method. In contrast to other methods where just a small amount (<1 g) of sample material is used, the gamma spectrometry requires a much larger sample amount (Preusser et al., 2008). For the NW09 core, 350-450 g material from each sample was needed to fill the gamma spectrometry sample containers.
For the final calculation of the dose rate, the results from radionuclide measurements are combined with the influence of cosmic radiation, deduced from latitude, longitude, height above sea level, sediment cover and sediment density and additional sample specific information about grain-size and moisture content. These complex dose rate calculations are accomplished with the software called ADELE (Age Determination for Luminescence and ESR), version 1.06 (Kulig, 2005).

4.7.9 Age calculation and uncertainty estimation

The age calculation is the final step in the dating process. When paleodose and dose rate determination are derived, the age of a sample can be calculated following equation [1]. All these calculations are carried out using again the ADELE software. For an adequate uncertainty estimation of the IRSL ages, the arithmetic mean and the standard error of the equivalent doses from all aliquots measured from one sample are calculated and are as well entered into the age calculation software.

5 Results

This chapter describes and presents the results of the different methods used. The information about the lithology of the NW09 core is followed by explanations about its geochemical and geophysical properties. A compilation of these results can be found in the appendix. With the information gained from the core description, a subdivision of the core into lithologic units will be possible. The results of luminescence dating, providing a detailed chronological classification, close the results from the NW09 core. A series of results from geochemical investigation on reference samples taken in the catchment area of the NW09 core will complete this chapter.

5.1 Lithology

The results of the sediment description are based on the analysis of the core from photographs, sketches and direct observations. The sediment core from Niederweningen covers a total length of 93.6 m. As the thesis mainly focuses on the transition from MIS 6 into 5e, only the sequence that was assumed to represent this transition was sketched in detail. Based on a comparison of the NW09 core with the results from previous projects in the Wehntal (see chapter 3), a section from the bottom, of what is assumed to be the Eemian peat, at 9.36 m down to 18.83 m depth was identified as the MIS 6 to 5e transition. More than two meters were added below and above this sequence to assure an appropriate placement to the sedimentological context of the core. Hence, the core section presented here reaches from 21-7 m in depth (Fig. 5-1).

Below the main sequence beginning at a depth of 18.83 m, a homogeneous succession of fine-grained sediment is present, reaching down to 44.50 m and consisting of grey clayey silts and silty clays. Further, a lamination of the sediment being attended by a change in colour from light- to dark-grey dominates this sequence (Fig. 5-1). The lamination frequently shows substantial deformation structures and therefore is only vaguely distinguishable. These deformations partially lead to a mottled sediment colour.

Above 18.83 m, a gradual change in sediment colour and grain-size can be noticed (Fig. 5-1). The colour changes from grey to light grey – brownish and even bluish layers (above 15 m). At the top of the transitional sequence from 10.50 to the beginning of the peat sequence at 9.36 m, a slightly greenish colour occurs. The change in grain-size involves the occurrence of coarser grain-sizes such as lenses of sandy

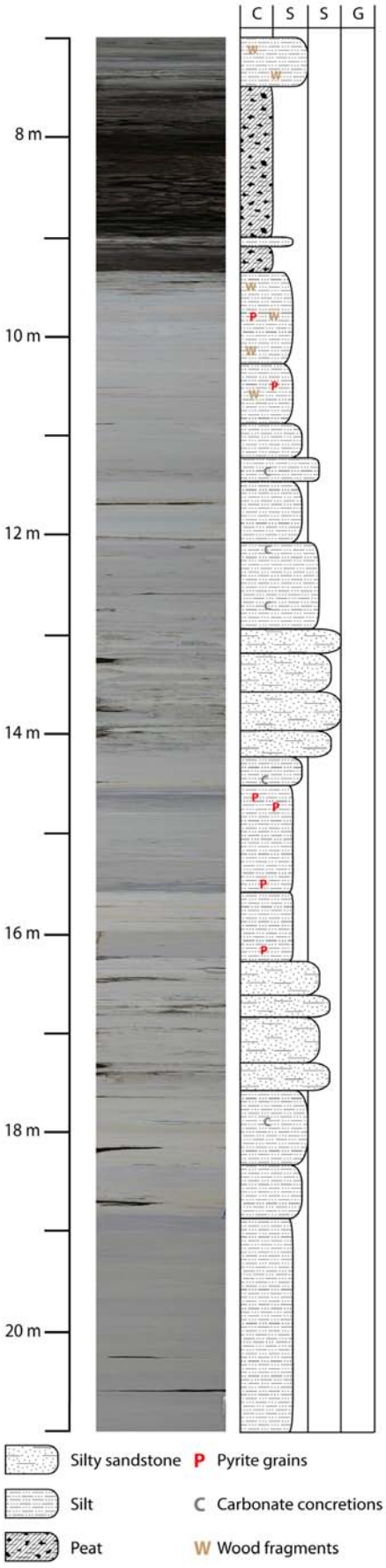

silts or even fine or medium sand, e.g. at 16.28-17.60 m. Further, two weakly consolidated sandstones were found in this band at 16.50 and 16.65 m. From 12.80-14.25 m, a sequence of medium to coarse sand with irregularly occurring silt layers dominates. Nevertheless, the clayey silts and silty clays remain the prevailing grain-sizes, building up the background grain-size signal of the core sequence between 18.83 and 9.36 m.

Besides these changes in colour and grain-size, there are three striking elements occurring in this transitional sequence: carbonate concretions, pyrite formation and organic material. The first occurrence of a carbonate concretion is at 17.85 m depth. Such concretions with diameters of <1 cm up to 5 cm were found up to the bottom of the peat horizon at 9.36 m. From a depth of 16.25 m, black striations were recognised. Smear slide analyses, using polarisation filters, identified diagenetic pyrite as main source of the blackish colour observed. Black striations and small grains (<1 mm) of pyrite are present up to 9.36 m. A first clear occurrence of organic material sets in at 14.78 m in form of small wood fragments. From 10.85 m up to the transition to the peat layer at 9.36 m, a considerable increase in the amount and dimension of the wood fragments was observed.

The peat horizon ranges from 9.36–7.55 m (Fig. 5-1). The transition, however, is not abrupt but with an increasing humus content starting at 9.60 m. A minor part of humous silts and clays remain in most parts of the peat. An almost pure peat was observed between 9.35-9.25 m and 8.25-8.00 m.

Figure 5-1: Core photograph from 7-21 m depth and lithology of the core sequence. The lithology classification (CSSG) is clay, silt, sand and gravel.

Above the peat horizon from 7.55-7.00 m, a rough lamination of green-brownish to grey sandy silts was observed. Some peat grains and wood fragments are still present, but their amount decreases towards the top of the section.

Based on this core description, nine major lithologic units divided into 18 different sequences can be distinguished from 21-7 m, as shown in Fig. 5-2. Lithologic units are labelled in capital letters. The subscripted numbers explain slight differences within the same major unit or a repetition of the same unit higher above in the core.

5.2 Grain-size distribution

The results from grain-size measurements coincide with the results from sediment description (Fig. 5-3). The core part below 18.83 m (unit A) is fine grained with a median grain-size of 6-8 µm resulting in a dominance of the silt fraction (2-63 µm).

For the sequence from 18.83-9.36 m, the grain-size distribution again shows a dominance of the silt fraction (60-80%). In parts dominated by sand lenses, the silt content decreases to ~30%. The clay fraction (<2 µm) only varies between 10-20%, whereas the sand fraction (63-2000 µm) varies much more due to the occurrence of the sand lenses mentioned above. These sandy layers lead to an increase of the sand content from an average value of 1-5% to >55% (at 17.50 m, unit D_1) or even >60% (at 16.80 and 13.80 m, unit D_1 and D_2). The median grain-size values above the transition at 18.83 m show a termination of the homogeneous grain-size conditions and follow the three sand fraction peaks in the units D_1 and D_2. The grain-size distributions of the samples measured in these sand lenses all reveal a bimodal grain-size distribution pattern, showing two peaks in the distribution curves (Fig. 5-4). One peak reflects the sandy fraction in the samples with a grain-size around 200 µm, whereas the smaller second peak shows the fine-grained background signal of 6-10 µm. In between and after these peaks, the median grain-size decreases to values from 6-10 µm and finally showing a slight, gradual increase throughout the peat layer ending up at values around 20 µm at 7 m depth.

5.3 Geochemistry

The results of geochemical investigations again show a clear change during the transitional sequence above 18.83 m depth. The homogeneous sequence between 44.50-18.83 m does not reveal any remarkable variations in TOC, TIC and $CaCO_3$ contents.

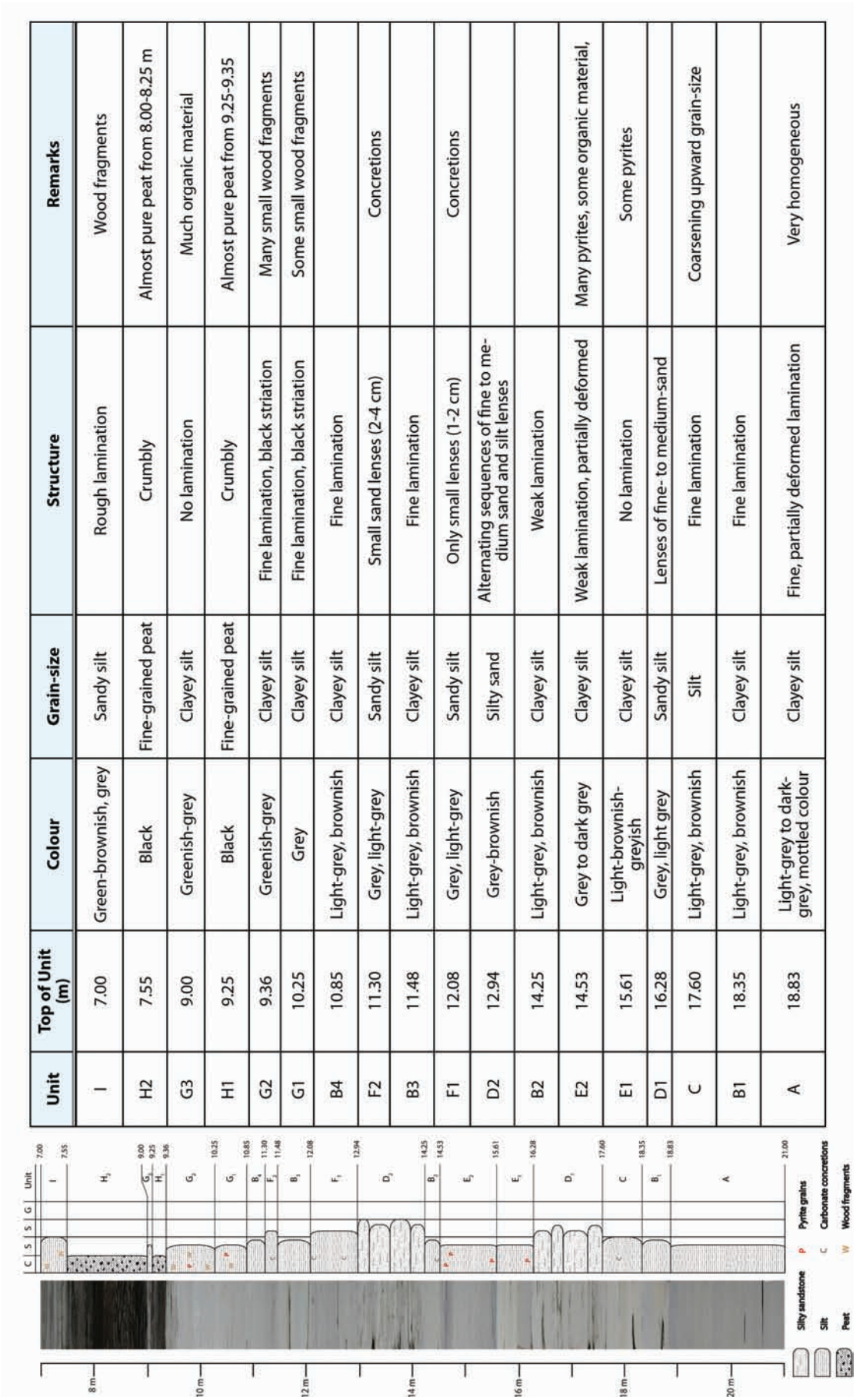

Unit	Top of Unit (m)	Colour	Grain-size	Structure	Remarks
I	7.00	Green-brownish, grey	Sandy silt	Rough lamination	Wood fragments
H2	7.55	Black	Fine-grained peat	Crumbly	Almost pure peat from 8.00-8.25 m
G3	9.00	Greenish-grey	Clayey silt	No lamination	Much organic material
H1	9.25	Black	Fine-grained peat	Crumbly	Almost pure peat from 9.25-9.35
G2	9.36	Greenish-grey	Clayey silt	Fine lamination, black striation	Many small wood fragments
G1	10.25	Grey	Clayey silt	Fine lamination, black striation	Some small wood fragments
B4	10.85	Light-grey, brownish	Clayey silt	Fine lamination	
F2	11.30	Grey, light-grey	Sandy silt	Small sand lenses (2-4 cm)	Concretions
B3	11.48	Light-grey, brownish	Clayey silt	Fine lamination	
F1	12.08	Grey, light-grey	Sandy silt	Only small lenses (1-2 cm)	Concretions
D2	12.94	Grey-brownish	Silty sand	Alternating sequences of fine to medium sand and silt lenses	
B2	14.25	Light-grey, brownish	Clayey silt	Weak lamination	
E2	14.53	Grey to dark grey	Clayey silt	Weak lamination, partially deformed	Many pyrites, some organic material,
E1	15.61	Light-brownish-greyish	Clayey silt	No lamination	Some pyrites
D1	16.28	Grey, light grey	Sandy silt	Lenses of fine- to medium-sand	
C	17.60	Light-grey, brownish	Silt	Fine lamination	Coarsening upward grain-size
B1	18.35	Light-grey, brownish	Clayey silt	Fine lamination	
A	18.83	Light-grey to dark-grey, mottled colour	Clayey silt	Fine, partially deformed lamination	Very homogeneous

Figure 5-2: Description of stratigraphic units deduced from sediment description.

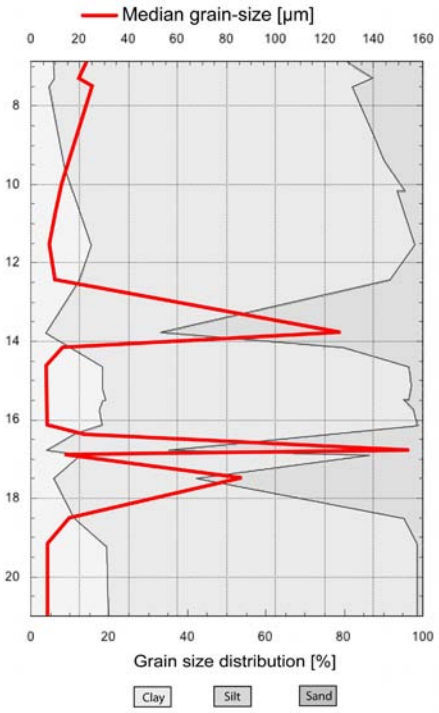

Figure 5-3: Median grain-size and grain-size distribution curve from grain-size measurement using the Malvern Mastersizer 2000 showing three sand peaks at 17.50, 16.80 and 13.80 m.

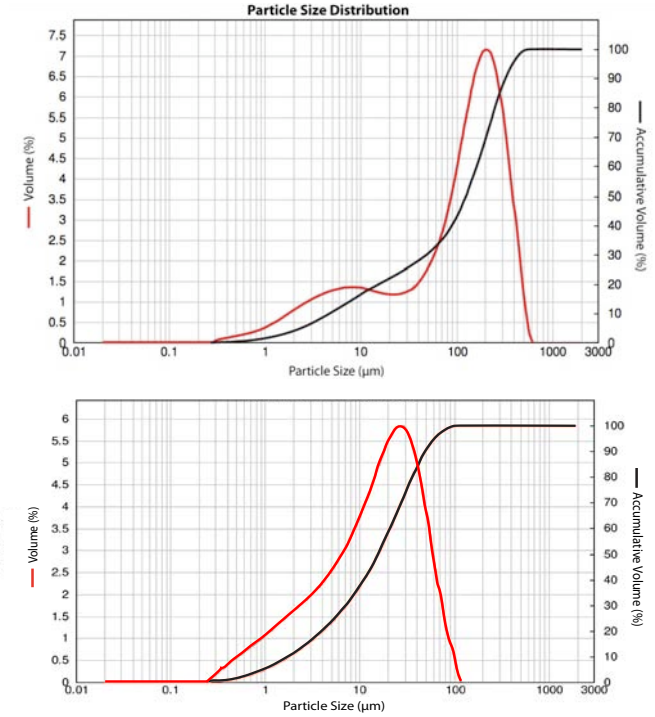

Figure 5-4: Upper picture: Bimodality of grain-size distribution from the sample at 13.80 m. The plateau around 6-10 µm reflects the fine-grained background signal, whereas the peak at ~200 µm shows the additional input of sandy material. A similar pattern can be noticed at 17.50 and 16.80 m depth. Lower picture: Grain-size distribution from 18.50 m depth showing already a slightly increasing grain-size below the first sand peak at 17.50 m.

The TOC shows stable results and very low values (mean = 0.37 ± 0.12 wt), whereas the carbonate content values are around 40-45 wt-% (mean = 43.95 ± 1.41 wt-%). As the $CaCO_3$ values are directly deduced from TIC values, the TIC results contain exactly the same characteristics as the carbonate values and therefore are not presented separately.

Contrary to the results revealed from sediment description, the geochemical investigations do not show a distinct change immediately after the transition at 18.83 m (Fig. 5-5).

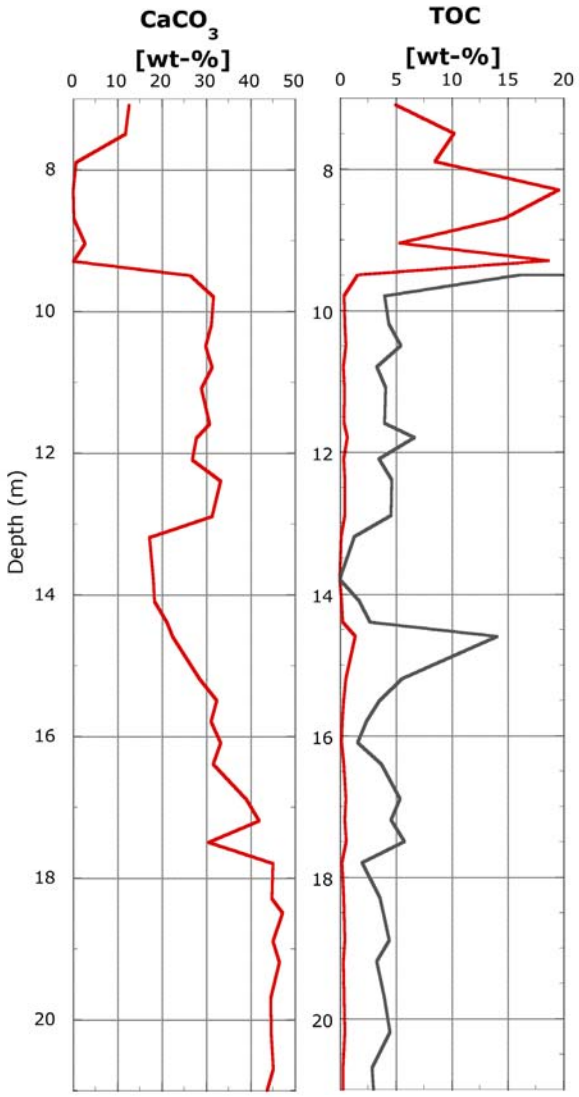

Figure 5-5: Results from geochemical analysis. Left side: $CaCO_3$ curve showing a gradual decrease in carbonate content. The decrease is little delayed and does not start simultaneously with the changes in colour and grain size at 18.83 m. Right side: TOC curve showing no general changes after the transition at 18.83 m, but indicates the appearance of wood fragments at 14.78 m. Black line shows exaggerated values by a factor of 10.

Despite a clearly visible decrease in the $CaCO_3$ content in the course of the transitional sequence from 18.83-9.36 m, the decreasing signal does not start synchronously with the changes in colour mentioned above. The first measurement of this sequence shows a high carbonate value of 47.27 wt-% at 18.50 m, before the $CaCO_3$ content starts to decrease. The gradual decrease between 18.50-13.20 m is interrupted by low carbonate values at 17.50 m (unit C), but then follows the previous decreasing pattern until 13.20 m, where the lowest $CaCO_3$ value of the transitional sequence of 17.31 wt-% is reached. From 13.20-9.50 m, a carbonate plateau with values fluctuating around 30 wt-% occurs, before the peat horizon leads to very low values with a mean of 0.82 wt-% in units I_1 and I_2.

The TOC content is in close relation with the presence of wood fragments in the core. Therefore, a first peak in TOC was observed synchronously with the first occurrence of wood pieces around 14.78 m. A second and much stronger increase in TOC was observed immediately before and during the peat sequence from 9.36-7.55 m. Due to the presence of a humous silt and clay layer within the peat sequence at 9.00-9 .25m (unit $G_{3)}$, the TOC shows a change towards lower TOC values (Fig. 5-5).

5.4 Geophysical properties

In the homogeneous part below the transition at 18.83 m, bulk density, magnetic susceptibility and shear strength show only very little variation (Fig. 5-6). The density values fluctuate around 2.1±0.2 g cm^{-3}, whereas the magnetic susceptibility values are very low ranging from 1.5-2.2. The fine-grained silty sequence leads to relatively high shear strength values of 1.0-1.2 N cm^{-2}.

The lowermost part of the transitional sequence immediately above 18.83 m (unit B_1 and C) does not reveal any differences in bulk density and magnetic susceptibility, compared to the part below. The shear strength, in contrast, shows a decrease to 0.65 N cm^{-2}, coinciding with the slight increase in grain-size at 18.65 m. Up-core, the shear strength generally follows the grain-size variations, leading to very low shear strength values of 0.1-0.2 N cm^{-2} in parts dominated by sandy sequences.
The magnetic susceptibility remains very stable showing only one part with increased values at 15.90-14.50 m (units E_1 and E_2). These elevated values of up to 70.0 coincide with the appearance of diagenetic pyrites.
The bulk density curve shows almost a similar stability with the exception of low-density values between 17.43-16.28 m (unit D_1) and 13.95-13.42 m (unit D_2). Disregarding these low-density peaks, a detailed observation of the curve reveals changes

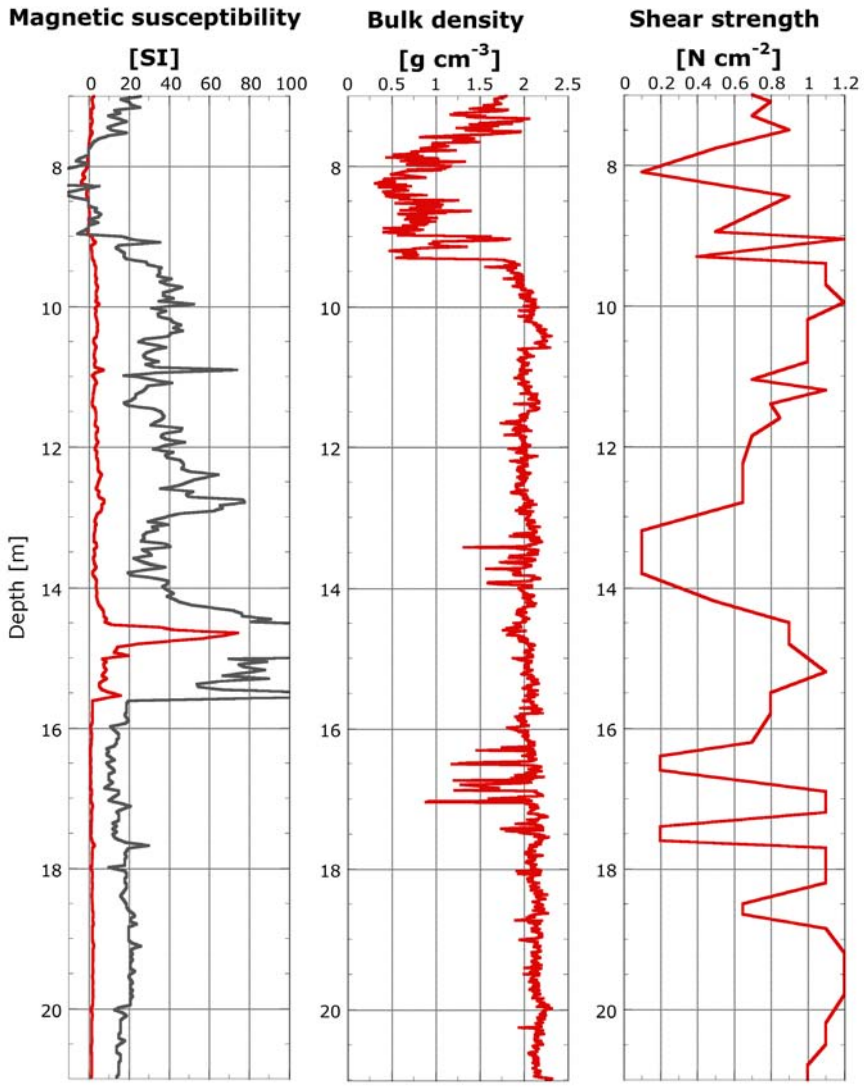

Figure 5-6: Plots showing geophysical properties of the NW09 core from 21-7 m. Left side: Magnetic susceptibility curve shows almost no variations except the peak between 14.50-15.00 m probably resulting from the appearance of pyrite formation in the sediment. Black line shows exaggerated values by a factor of 10. Middle: Bulk density curve showing only very little variation, except from the decrease during the peat layers. Right side: Sear strength curve generally follows the variations in grain-size.

in the mean density below and above the low values in unit D_1 from 2.14 g cm^{-3} (at 21.00-17.44 m) to 2.03 g cm^{-3} (at 16.26-13.96 m). The peat layers above 9.36 m (units I_1 and I_2) lead to decreasing shear strength, bulk density and magnetic susceptibility values.

5.5 Palynology

Although the palynological investigations are done by Dr. Ruth Drescher-Schneider and are not completed yet, some intermediate results are shortly presented here, in order to support the interpretation of the NW09 core section.

The pollen analysis shows a conspicuous rise in the pollen concentration for the sequence from 18.83-9.36 m in comparison to the sequence below, accompanied by a gradual climate enhancement. A dominance of non-tree pollen can be noticed, with some sequences of pollen from *Betula* (birch) and *Pinus* (pine). At the beginning of the peat horizon in unit H_1, an abrupt onset of *Alnus* (alder) vegetation can be noticed (Drescher-Schneider, unpublished data).

5.6 IRSL Dating

The results from IRSL dating include data from all the 24 samples taken, as all the samples were part of the measurement analysis process and due to better interpretation possibilities.

5.6.1 Test results

Prior to the analysis of the equivalent dose measurements, the results from the testing procedure were analysed. The results from the dose recovery test show a ratio of the reovered/given dose between 0.97 and 1.13 (Table 5-1), whereas a value of 1.00 would be ideal. The precision of the dose recovery test is highly dependent on the luminescence properties of the samples (Preusser et al., 2007). The mean relative standard deviation of 2.7% of the recovered doses indicates a good precision compared to values between 10-15% found for glacial deposits from Switzerland (Preusser et al., 2007). Further, two preheat tests were carried out on the sample NWE18, which revealed an ideal preheat temperature of 270°C (see Fig. 4-7). Therefore, this preheat temperature was applied for all samples of the NW09 core (NWE1-24).

Preheat temperature (°C)	Number of Aliquots	Recovered mean dose (Gy)	RSD (%)	Ratio recovered / given dose
230	3	440.2 ± 5.4	0.8	1.03
250	3	473.6 ± 7.4	3.1	1.11
270	3	481.1 ± 9.6	0.6	1.13
290	3	437.6 ± 9.7	1.3	1.03
310	2	412.0 ± 13.6	7.4	0.97

Table 5-1: Results of combined dose-recovery and preheat test on sample NWE18. The laboratory dose induced was 426.4 Gy (=4000 s β-source irradiation). RSD is the Relative Standard Deviation. For an ideal procedure, the ratio of recovered/given dose is close to 1.00.

The fading test was carried out, to check whether the IRSL signal is affected by anomalous fading or not. This test was again accomplished on the sample NWE18 and the results revealed a significant fading with a mean g-value (fading rate) of 2% per decade (Table 5-2). This value is within an expected fading rate of 4-6% per decade for polymineral fine-grain IRSL measurements of young samples (<40-50 ka)(Zink, 2008). As all the samples measured are from the same sediment core, the fading rate was conferred to all other samples and the fading correction after Lamothe et al. (2003) had to be applied after the age calculation to unfade the calculated ages.

Sample	g-value
NWE18 a	0.015
NWE18 b	0.020
NWE18 c	0.015
NWE18 d	0.032
Mean :	**0.02**

Table 5-2: Results of the fading test applied on four different aliquots of the sample NWE18, revealing a mean fading rate (g-value) of 2% per decade.

5.6.2 Evaluation and selection of the D_e results

The Luminescence Analyst software automatically generates an exponential growth curve for each aliquot measured and calculates the resulting D_e values. As the signal intensity decreases over time, only a certain integral at the beginning of the detection time was taken into account. Equally, an integral at the end of the detection time was chosen as background signal and was subtracted from the signal measured during the first integral (Fig. 5-7). To assure consistent measurements, the stimulation time, detection integral and background integral were chosen constant as shown in Table 5-3.

Sample	Stimulation time	Signal integral	Background integral
NWE1-24	300 s	1-25 s	250-300 s

Table 5-3: Table showing the evaluation parameters selected for all samples of the NW09 core.

For reliable results, only the D_e values from the aliquots that passed the internal tests in the SAR protocol (recuperation- and recycling ratio) were included in the data analysis. Table 5-4 shows the results from all D_e measurements using IRSL. Recuperation and recycling ration were in an acceptable range for all aliquots, except one from NWE1 and one from NWE17.

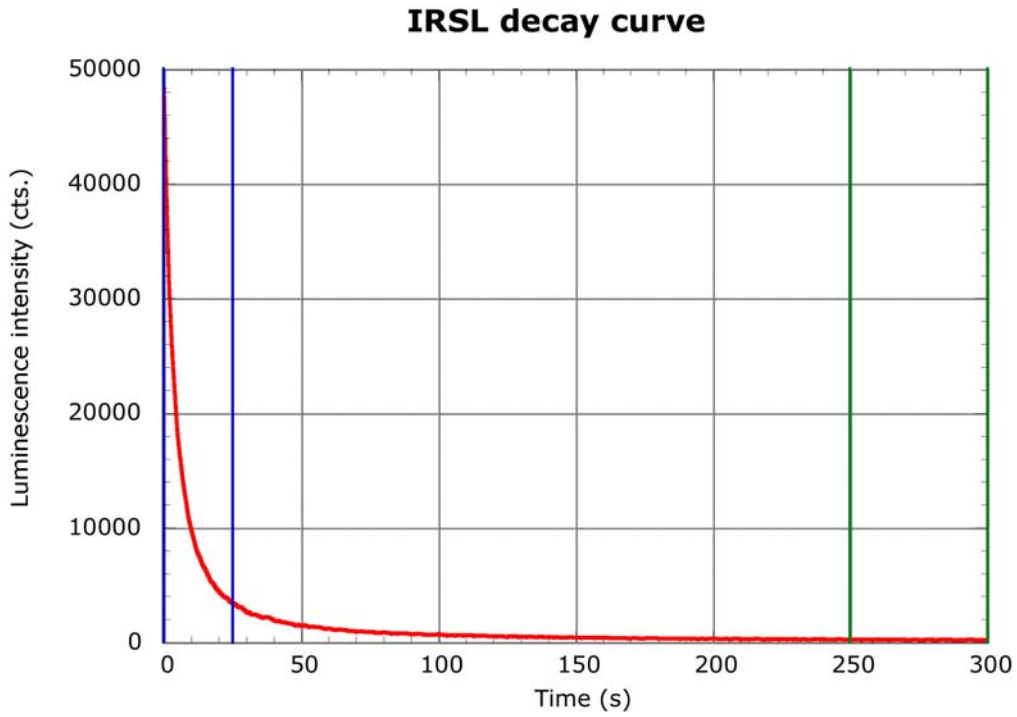

Figure 5-7: Result of the IRSL signal measured on sample NWE17. Blue lines show time integral considered for the D_e measurement (0-25 s) and green lines show time integral taken for the evaluation of the background signal (250-300 s).

5.6.3 Dose rate results

The results of the dose rate determination are presented in Table 5-5. For the calculation of the external dose rate, the water content of the sediment is needed. Although the present water content was measured during the sample preparation, a uniform moisture content of 30±5 % was selected for all samples as an estimation of the primary conditions. For the calculation of the internal dose rate, the amount of potassium in the feldspars is needed. As in the laboratory, only a separation of potassium rich feldspars and not of pure potassic feldspars is possible, an empirically determined standard value of 12.5±0.5 % was taken, as proposed by Huntley and Baril (1997).

5.6.4 IRSL ages

The final results of the IRSL ages before and after the fading correction are shown in Table 5-6. Fig. 5-8 shows the unfaded ages in relation with the core depth. The IRSL ages from the NW09 core reach from ~300 ka at the bottom to ~50 ka in the upper part of the core. The age/depth model from Fig. 5-8 reveals a more or less continuous increase of the ages with depth, however, with a few exceptions.

The samples NWE9 and NWE10 are more than 100 ka older than the ones from

the over- and underlying samples. Furthermore, there is a gap in the chronology between the samples NWE17 and NWE18, which is exactly at the beginning of the transitional sequence at 18.83 m depth. The samples of the transitional sequence from 18.83-9.36 m (NWE18-NWE22) revealed very similar ages and are hardly distinguishable within their error bars.

Sample	Aliquots selected/ measured	Mean recycling ratio	Mean recuperation (%)	Mean D_e (Gy)	Standard error (Gy)
NWE1	2/3	0.93	<5	812.0	55.8
NWE2	3/3	0.99	<5	586.2	13.3
NWE3	3/3	0.99	<5	515.3	5.8
NWE4	3/3	0.97	<5	536.4	8.5
NWE5	3/3	0.99	<5	542.6	7.7
NWE6	3/3	0.95	<5	601.5	3.7
NWE7	3/3	0.98	<5	507.8	16.3
NWE8	3/3	1.02	<5	487.8	13.3
NWE9	3/3	0.94	<5	646.6	23.0
NWE10	5/5	0.95	<5	535.8	27.5
NWE11	5/5	1.01	<5	486.4	19.8
NWE12	3/3	0.99	<5	507.6	4.1
NWE13	5/5	0.98	<5	463.0	22.2
NWE14	5/5	0.98	<5	551.8	21.6
NWE15	5/5	0.99	<5	455.3	27.8
NWE16	5/5	1.00	<5	449.3	25.2
NWE17	4/5	0.98	<5	429.3	14.1
NWE18	3/3	0.97	<5	349.0	3.0
NWE19	3/3	0.96	<5	358.4	4.1
NWE20	3/3	0.93	<5	301.7	2.9
NWE21	3/3	0.92	<5	351.7	3.0
NWE22	3/3	0.99	<5	292.5	1.3
NWE23	3/3	0.97	<5	132.3	2.6
NWE24	3/3	0.99	<5	130.3	2.8

Table 5-4: Results of all equivalent dose (D_e) measurements, including results from recuperation and recycling ratio test. For reliable data, the recycling ratio has to be in the range of 0.9-1.1 and a recuperation value of <5% has to be reached, which is the case for all samples.

Sample	Depth (m)	K (%)	Th (ppm)	U (ppm)	M (%)	W (%)	Dose rate (Gy ka^{-1})
NWE1	91.45	2.87 ± 0.03	10.94 ± 0.19	2.20 ± 0.05	7.3	30 ± 5	**3.74 ± 0.48**
NWE2	86.45	1.22 ± 0.01	6.44 ± 0.08	2.63 ± 0.06	14.3	30 ± 5	**2.27 ± 0.24**
NWE3	80.6	1.18 ± 0.01	6.88 ± 0.14	2.49 ± 0.08	17.7	30 ± 5	**2.24 ± 0.23**
NWE4	77.8	1.11 ± 0.01	6.14 ± 0.14	2.48 ± 0.06	24	30 ± 5	**2.12 ± 0.22**
NWE5	73.85	1.16 ± 0.01	7.09 ± 0.13	2.57 ± 0.03	19.2	30 ± 5	**2.27 ± 0.23**
NWE6	69.41	1.17 ± 0.01	6.09 ± 0.29	2.46 ± 0.02	17.1	30 ± 5	**2.16 ± 0.22**
NWE7	60.36	1.29 ± 0.02	6.89 ± 0.21	2.35 ± 0.04	16.8	30 ± 5	**2.28 ± 0.25**
NWE8	53.71	1.30 ± 0.01	6.94 ± 0.22	2.42 ± 0.02	19.8	30 ± 5	**2.31 ± 0.24**
NWE9	48.53	1.20 ± 0.01	5.79 ± 0.39	2.17 ± 0.03	21.7	30 ± 5	**2.07 ± 0.24**
NWE10	45.31	1.06 ± 0.01	4.67 ± 0.12	1.91 ± 0.03	24.4	30 ± 5	**1.79 ± 0.22**
NWE11	40.3	1.40 ± 0.02	7.42 ± 0.30	2.45 ± 0.09	19	30 ± 5	**2.44 ± 0.28**
NWE12	38.5	1.34 ± 0.02	7.40 ± 0.15	2.47 ± 0.05	19.1	30 ± 5	**2.40 ± 0.24**
NWE13	35.23	1.38 ± 0.02	7.39 ± 0.17	2.35 ± 0.09	20	30 ± 5	**2.40 ± 0.29**
NWE14	32.46	1.34 ± 0.02	7.40 ± 0.20	2.51 ± 0.04	19.6	30 ± 5	**2.42 ± 0.27**
NWE15	29.25	1.34 ± 0.02	7.21 ± 0.15	2.37 ± 0.09	18.6	30 ± 5	**2.37 ± 0.31**
NWE16	24.27	1.47 ± 0.02	7.52 ± 0.31	2.42 ± 0.05	19.4	30 ± 5	**2.50 ± 0.32**
NWE17	19.55	1.32 ± 0.02	7.53 ± 0.09	2.43 ± 0.02	18.4	30 ± 5	**2.41 ± 0.26**
NWE18	16.2	1.72 ± 0.02	9.04 ± 0.15	3.11 ± 0.03	22.7	30 ± 5	**3.04 ± 0.30**
NWE19	14.89	2.11 ± 0.02	10.81 ± 0.37	3.47 ± 0.09	22.6	30 ± 5	**3.59 ± 0.36**
NWE20	12.49	1.77 ± 0.02	8.16 ± 0.24	2.55 ± 0.04	24.7	30 ± 5	**2.85 ± 0.27**
NWE21	11.55	1.80 ± 0.02	8.70 ± 0.18	2.54 ± 0.02	22.8	30 ± 5	**2.92 ± 0.28**
NWE22	10.57	1.78 ± 0.02	8.75 ± 0.25	2.30 ± 0.04	23.4	30 ± 5	**2.85 ± 0.27**
NWE23	5.65	1.76 ± 0.02	9.86 ± 0.26	2.48 ± 0.03	30.9	30 ± 5	**3.03 ± 0.30**
NWE24	3.5	1.81 ± 0.02	9.66 ± 0.35	2.65 ± 0.07	30.3	30 ± 5	**3.12 ± 0.32**

Table 5-5: Results from dose rate determination. U, Th and K values were converted after the gamma spectrometry using conversion factors a Adamiec and Aitken (1998). M is the moisture content measured in the laboratory during sample preparation and W is the estimated primary water content used for the dose rate calculation.

Sample	Age (ka)	Age unfaded (ka)
NWE1	217.3 ± 23.7	**259.60 ± 28.34**
NWE2	258.0 ± 26.3	**308.77 ± 31.51**
NWE3	230.0 ± 23.6	**274.93 ± 28.24**
NWE4	253.3 ± 26.0	**303.09 ± 31.14**
NWE5	239.5 ± 24.4	**286.41 ± 29.21**
NWE6	278.8 ± 28.3	**333.93 ± 33.93**
NWE7	222.5 ± 23.0	**265.87 ± 27.51**
NWE8	210.9 ± 21.5	**251.87 ± 25.71**
NWE9	312.3 ± 33.7	**374.50 ± 40.45**
NWE10	299.3 ± 32.5	**358.75 ± 38.99**
NWE11	199.2 ± 21.7	**237.76 ± 25.93**
NWE12	211.5 ± 20.9	**252.60 ± 24.99**
NWE13	193.3 ± 21.4	**230.64 ± 25.56**
NWE14	227.9 ± 24.2	**272.39 ± 28.95**
NWE15	192.5 ± 22.5	**229.68 ± 26.87**
NWE16	179.6 ± 20.4	**214.13 ± 24.34**
NWE17	178.2 ± 18.3	**212.45 ± 21.84**
NWE18	114.7 ± 11.1	**136.12 ± 13.19**
NWE19	99.7 ± 9.9	**118.15 ± 11.75**
NWE20	105.8 ± 10.0	**125.46 ± 11.87**
NWE21	120.4 ± 11.3	**142.96 ± 13.43**
NWE22	102.8 ± 9.6	**121.86 ± 11.40**
NWE23	43.7 ± 4.3	**51.35 ± 5.06**
NWE24	41.7 ± 4.2	**48.98 ± 4.94**

Table 5-6: Results of the calculated IRSL ages before and after fading correction.

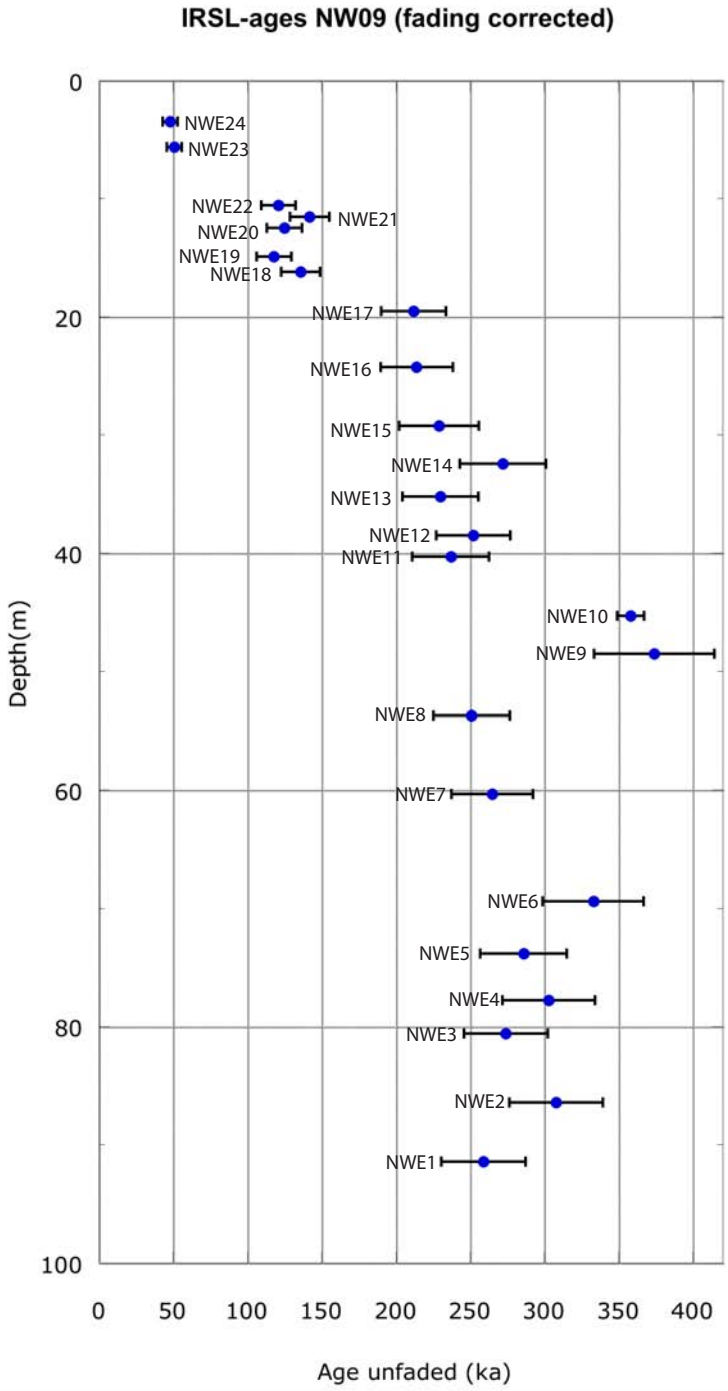

Figure 5-8: Results of IRSL dating plotted versus depth. Age/depth model showing the fading corrected ages of all NW09 samples.

5.7 Reference samples

After the measurements and a first observation of the samples from the NW09 core, the idea came up to take recent reference samples from the catchment area in order to have additional information for the placement and interpretation of the core samples. Therefore, a series of fine-grained samples from the river Glatt, one sample from the river Surb and several samples from Lake Zurich were taken for a carbonate analysis. The samples from Lake Zurich originate from cores taken for a past project of the ETH Zurich and are of late-glacial age (Strasser and Anselmetti, 2008). Detailed information about their position, age and geophysical properties can be found in Strasser and Anselmetti (2008). The carbonate measurements were conducted at the EAWAG in Dübendorf.

The results of the carbonate measurements and the detailed sampling locations of the Glatt and Surb samples are presented in Table 5-7. The Lake Zurich samples revealed a mean $CaCO_3$ content of 31.8 wt-%, whereas the samples from the River Glatt showed a much higher mean carbonate content of 43.4 wt-%. As only one sample from the river Surb was taken, the result is not representative, but at least revealed an approximation value of 33.7 wt-%.

Sample	Location (WGS84 coordinates)	$CaCO_3$ (wt-%)	Mean	Standard deviation
Glatt1	47.322 N / 8.708 E	41.8		
Glatt2	47.379 N / 8.646 E	56.7		
Glatt3	47.515 N / 8.519 E	41.4	**44.6**	6.7
Glatt4	47.524 N / 8.519 E	37.1		
Glatt5	47.573 N / 8.477 E	45.9		
Surb	47.501 N / 8.340 E	33.7	**33.7**	
ZHK04-4 0.4m	47.151 N / 8.899 E	22.2		
ZHK04-4 0.8m	47.151 N / 8.899 E	24.4		
ZHK04-5 0.4m	47.130 N / 8.452 E	39.7		
ZHK04-5 0.8m	47.130 N / 8.452 E	39.5	**31.8**	6.8
ZHK04-6 0.4m	47.146 N / 8.406 E	39.9		
ZHK04-6 0.8m	47.146 N / 8.406 E	26.5		
ZHK04-7 0.4m	47.163 N / 8.363 E	33.0		
ZHK04-7 0.8m	47.163 N / 8.363 E	29.0		

Table 5-7: Results of the reference samples from the rivers Glatt and Surb and from the Lake Zurich.

6 Interpretation and discussion

In the following chapter, the results presented above are interpreted and discussed with the focus on two main issues. The first one deals with the paleo-environmental evolution based on the IRSL ages in combination with the sedimentation history. The second main issue covers the interpretation of the geophysical and geochemical results concerning the depositional environment of the different units.

6.1 Paleo-environmental history

This chapter includes the interpretation and the discussion of the dating results from the whole NW09 core. Based on the IRSL ages, sedimentological observations of the whole core (done by Hans Axel Kemmna) and a placement of the samples in the context of the isotopic event stack after Bassinot et al. (1994), a paleo-environmental chronology of the NW09 core was generated (Fig. 6-1). Therefore, the core was divided into the following sequences: a sequence of Molasse and lodgement till is followed by a long sequence of lacustrine clay, containing dropstones and a second section of lacustrine clay without dropstones. Further up-core, the lacustrine sediments (units A-G), analysed in detail in this thesis, the peat of units H_1 and H_2 and finally, post Eemian lacustrine sediments and the mammoth peat follow. The present chapter tries to reconstruct the climatic conditions and changes leading to the different sequences from Fig. 6-1.

The lowermost luminescence sample NWE1 was taken in the Molasse sequence and showed a mean age of 260 ka, which is slightly younger than the age from the samples above, but still within their error range. Concerning the project's research question about the time of the valley formation, this age would propose a glacial erosion down to the Molasse during MIS 8. Whether this glacier advance during MIS 8 was responsible for the overdeepening of the Wehntal or the valley formation already took place during an earlier ice age remains uncertain. The hypothesis of an overdeepening during MIS 8, however, would support the general assumption of a glacial overdeepening during a Mid-Pleistocene ice age (Hantke and Wagner, 2004). Penck and Brückner (1909) suggested a formation of the Alpine valleys during the early Riss glacial stage, which probably corresponds to MIS 6 (Ehlers and Gibbard, 2007; Dehnert et al., 2010). Schlüchter (1987), however, suggested an age of at least one glacial cycle earlier than the Riss glacial (Hantke and Wagner, 2004), which would be MIS 8 or older and hence, in the age range of NWE1. A final conclusion concerning the age of the formation of the Wehntal, however, is not possible.

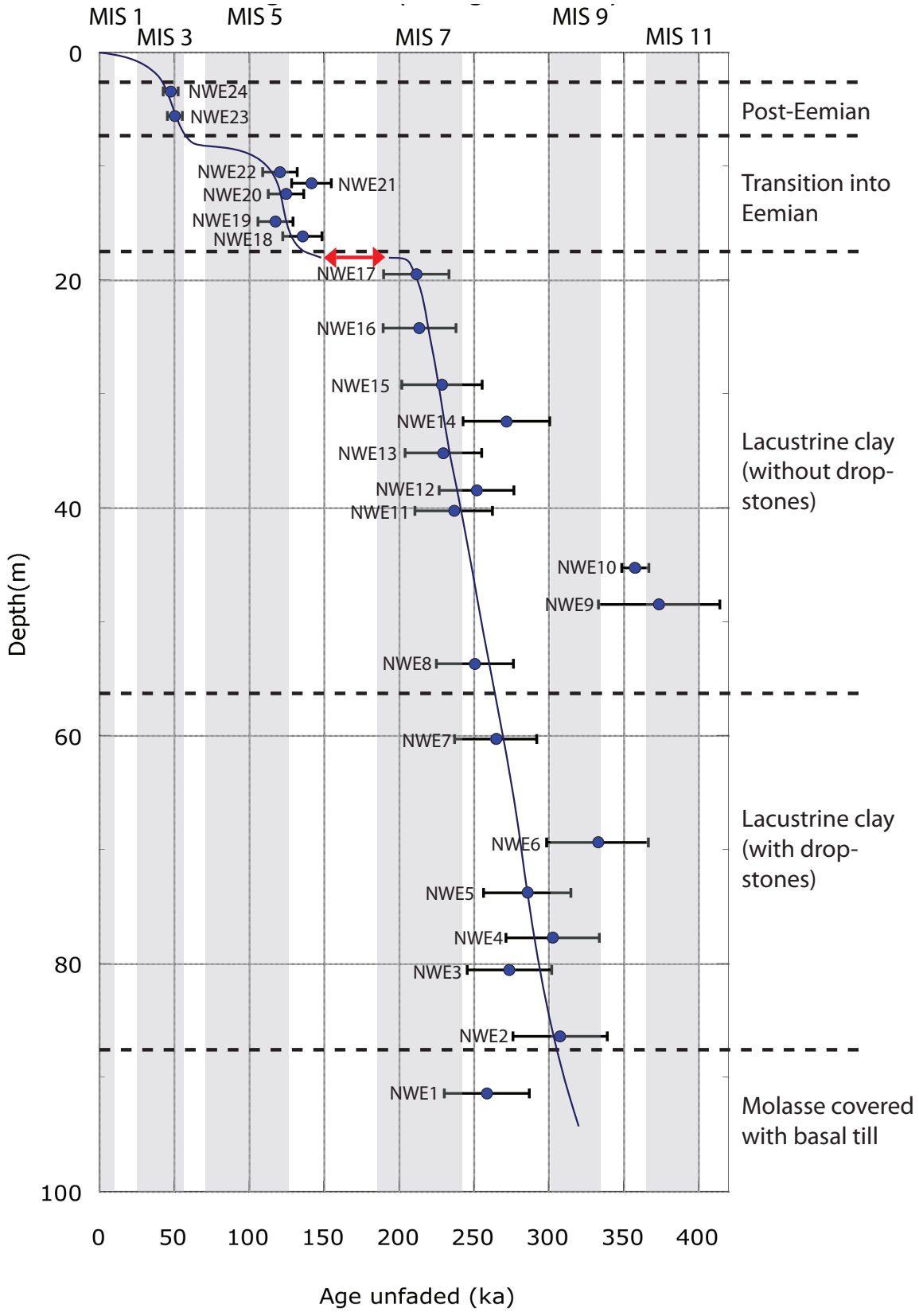

Figure 6-1: Combination of the fading corrected IRSL ages and sedimentological observations of the whole NW09 core. The red arrow marks a possible gap during MIS 6.

During the phase of the first lacustrine clay, the IRSL ages of the samples NWE2–NWE7 revealed mean ages from 334-266 ka, which correspond to the MIS 8 glacial. The presence of dropstones in this sequence supports the findings of a deposition during the MIS 8 glacial and is a clear evidence for stating the lake in the Wehntal as a proglacial lake. Consequently, the position of the glacier must have been close to the valley, causing calving icebergs and the deposition of dropstones at the drilling location.

For the second sequence of lacustrine clay, the IRSL ages of the sample NWE8-NWE17 show mean ages of 272-212 ka and therefore can be placed in the MIS 7 interglacial or slightly beyond. The lack of dropstones in this sequence is an indicator for a retreat of the glacier. The facts that glaciers are very sensitive to temperature changes (Ehlers, 1996) and that the sequence was dated as MIS 7 support the option of a retreating glacier. Except for the samples NWE9 and NWE10, the IRSL ages show a constant gradient within their error ranges. This can be interpreted as an indicator for a continuous sedimentation and an undisturbed sediment sequence. The ages of NWE9 and NWE10 are far beyond all the other ages measured and seem to be overestimated. A possible explanation for the overestimation may be the fact that both samples were taken from sandy layers. These units may originate from events with high transport-energies, leading to a short exposure-time to daylight, a high suspension load in the water and hence, to incomplete bleaching of the minerals before and during the deposition.

For the following section of lacustrine clays from units A-G_2, the IRSL measurements of the samples NWE18-NWE22 show an age range of 143-118 ka. Taking into account the uncertainty of the ages (see Table 5-6) of approximately 10%, they are representing the transition from MIS 6 into MIS 5e (Eemian interglaical). Comparing these ages with the ones from the sequence below, a hiatus of approximately 70 ka, including most of the MIS 6, can be observed between the samples NWE17 and NWE18, within only 3.35 m. As a change in colour and grain-size can be observed at 18.83 m (between unit A and B_1), perhaps representing an unconformity, a possible explanation for the hiatus would be a glacier advance during MIS 6 into the Wehntal, eroding the material deposited during this 70 ka and leading to this lack of sediment. That would be a possible option, if there were any marks of an advancing glacier in the dataset. The investigations, however, did not reveal any signs for glacial erosion in the dataset, except a slight increase in shear strength from 19.80-19.20 m (see Fig. 5-6). Another option for the observed discontinuity could be a glacier that was frozen on the lake bed and hence did hardly leave any other marks than the increasing shear strength (Ehlers, 1996). For such a glacial advance, however, the

unconformity seems far too unarticulated. An alternative hypothesis leading to a less articulated unconformity would be a swimming glacier, isolating the lake from any additional input and thus leading to a lack of sediment. This would be possible, if the sub- and supraglacial material was deposited elsewhere in the lake after the melting of the swimming glacial ice and icebergs. Besides the options assuming a glacier advance during MIS 6, there is also the possibility of cold conditions but no advance of the glacier into the Wehntal, causing a lack in the sediment. This lack of sediment would then be explained by minimal input from the catchment area of the lake leading to very low sedimentation rates. This hypothesis of ice free conditions in the Wehntal during MIS 6 is supported by Wyssling (2008), who suggested that the Glatt valley to the east of Niederweningen was probably not covered with ice, as the glacier did not get over the ridge at Hombrechtikon. This proposition, however, differs considerably from the statement of Buxtorf (1957), suggesting a massive glaciation during the Riss glaciation, which probably corresponds to the MIS 6, as mentioned above. Although the moraines of this glaciation are missing, the extent of the glaciation can be reconstructed by the occurrence of basal lodgement till and erratic boulders (Buxtorf, 1957). Based on these reconstructions, the MIS 6 glaciation may have reached the northern border of Switzerland at Schaffhausen and Konstanz and even further to the north (Buxtorf, 1957). Moreover, the dating of the penultimate glaciation erratic boulder by Graf et al. (2007), mentioned in chapter 3.2 is another evidence for a massive glaciation during MIS 6. These facts rather support the existence of a glacier in the Wehntal during MIS 6 and hence, an explanation of the hiatus based on a glacial impact.

Another possibility to explain the time lag could be caused by problems in the age determination. The most probable error in this case, again, would be incomplete bleaching of the samples below the hiatus (NWE7-NWE17), due to the turbid melt water of the proglacial lake.
For the age interpretation of the entire section above the discontinuity from units B_1-G_2, the results from Fig. 6-1 show that the IRSL ages of the samples NWE18-NWE22 are all very similar and hence, there is not much time included in this whole transitional sequence. This leads to the interpretation of a quite fast transition from MIS 6 into MIS 5e, despite the lack of a detailed chronology. For a more detailed interpretation of the transition, a higher IRSL sample density would be needed. Another fact complicating the temporal reconstruction of the transition is represented by the abrupt onset of *Alnus* pollen to ~25% at the beginning of the peat unit H_1, representing a hiatus between the units G_2 and H_1 (Drescher-Schneider, unpublished data). As there are hardly any investigations concerning the velocity of the MIS 6-5e transition for Switzerland, the isotopic event stack of Bassinot et al. (1994) was taken into ac-

count. The dataset as well shows a quite fast transition from MIS 6-5e of ~6 ka and hence, supports the hypothesis deduced from the IRSL ages of the NW09 core.
The uppermost two IRSL samples (NWE23 and NWE24) originate from a sequence of lacustrine sediments between the Eemian peat and the mammoth peat and revealed mean ages of 51-49 ka. These ages coincide with results from previous projects in Niederweningen, which dated the mammoth peat to ~45 ^{14}C ka BP (Hajdas et al., 2007) and hence, represent an independent age controll for the luminescence ages. The occurrence of lacustrine sediments probably reflects a period of re-flooding (Kemmna et al., unpublished data; Dehnert et al., unpublished data).

One important issue concerning the interpretation of the IRSL ages is their reliability. As already mentioned, the fact that the calculated ages show a quite consistent increase with depth is an evidence for a reliable age determination. Moreover, the justification for the outlying values NWE9 and NWE10 and the accordance of the ages from NWE18-NWE22 compared to palynological analysis for the pre-Eemian period (Drescher-Schneider, unpublished data) confirm the reliability of the ages. Nevertheless, there are still possible sources of errors, which could argue against the reliability of the IRSL ages. One issue concerning the samples from this core is the anomalous fading and the associated fading correction. As the testing procedure for the detection of anomalous fading was carried out only on one sample, the fading rate had to be adopted by all other samples. Although the samples are all from the same location, the different samples could hold different fading rates. To diminish this source of error, every sample should be tested on anomalous fading, which would be quite time-consuming. Another possible source of error has already been discussed above and concerns the phenomenon of incomplete bleaching during the transport and sedimentation process. Besides the sandy layers possibly originating from high transport-energy events (e.g. NWE9 and NWE10), also sediments deposited during a glacial period, characterised by a high amount of suspension load in the melting water leading to a shielding from light, could be affected by incomplete bleaching. The samples NWE2-NWE7 may show this effect, as the occurrence of dropstones is an evidence for the proximity of the glacier and an associated higher impact of turbid melt water. Nevertheless, a comparison with the samples above (NWE11-NWE17) shows a gradual progression of the IRSL ages and hence, probably do not reveal an overestimation due to incomplete bleaching.

6.2 Environmental conditions during deposition at the MIS 6-5e transition

In order to merge all the information from the different datasests and for an interpretation of the depositional environment of the sediment, the core sequence from 21-7 m was subdivided into 'depositional units', less detailed than the lithologic units from Figure 5-2 (Fig. 6-2). This less detailed subdivision is based on observations showing that the lithologic units from sediment description show more detailed characteristics than the data from geophysical and geochemical investigations. For a reconstruction of the depositional environment, however, these datasets are the main source of information and therefore, this less detailed subdivision seems feasible. Nevertheless, the lithologic units are still included in the discussion.
The following interpretation is mainly focused on two variables, namely the grain-size and carbonate content values, as most of the variations in one of the other variables can be deduced or at least be apparent in one of these two datasets. To assure that grain-size and carbonate values are independent from each other and hence contain different information, a correlation analysis was carried out. Thereby, the carbonate values were plotted separately against various grain-size fractions (clay, silt, fine-sand and sand) and against the median grain-size values. None of the samples showed significant correlation as can be deduced from the determination coefficients in Table 6-1. Therefore, the carbonate values seem not to be coupled to the grain-size signal, reflecting mainly the system's transport energy.

Variables	Determination coefficient (R^2)
CaCO3 vs. Clay (<2 µm) content	0.16
CaCO3 vs. Silt (2-63 µm) content	0.21
CaCO3 vs. Sand (63-2000 µm) content	0.22
CaCO3 vs. Fine-sand (63-250 µm) content	0.17
CaCO3 content vs. Median grain-size	0.16

Table 6-1: Correlation analysis between CaCO3 content and different grain-size fractions. The determination coefficients shwo all values far below a significant correlation.

The first one of these depositional units (Dep-1) reaches from the bottom of the core sequence at 21.00 up to 17.60 m (units A, B_1 and C), where the $CaCO_3$ content starts to decrease. The reason for choosing the threshold according to the changing carbonate values and not to the shifting grain-size and sediment colour at 18.83 m is based on statistical tests. Thereby, the *Welch Two Sample t-test* was applied to deduce significant changes in the means before and after the transition. As the conditions below 21.00 m stay very stable for both, grain-size and carbonate, the datasets for the testing procedure were expanded with the values down to 44.50 m. The results only revealed a significant difference in the means for the carbonate values, albeit on

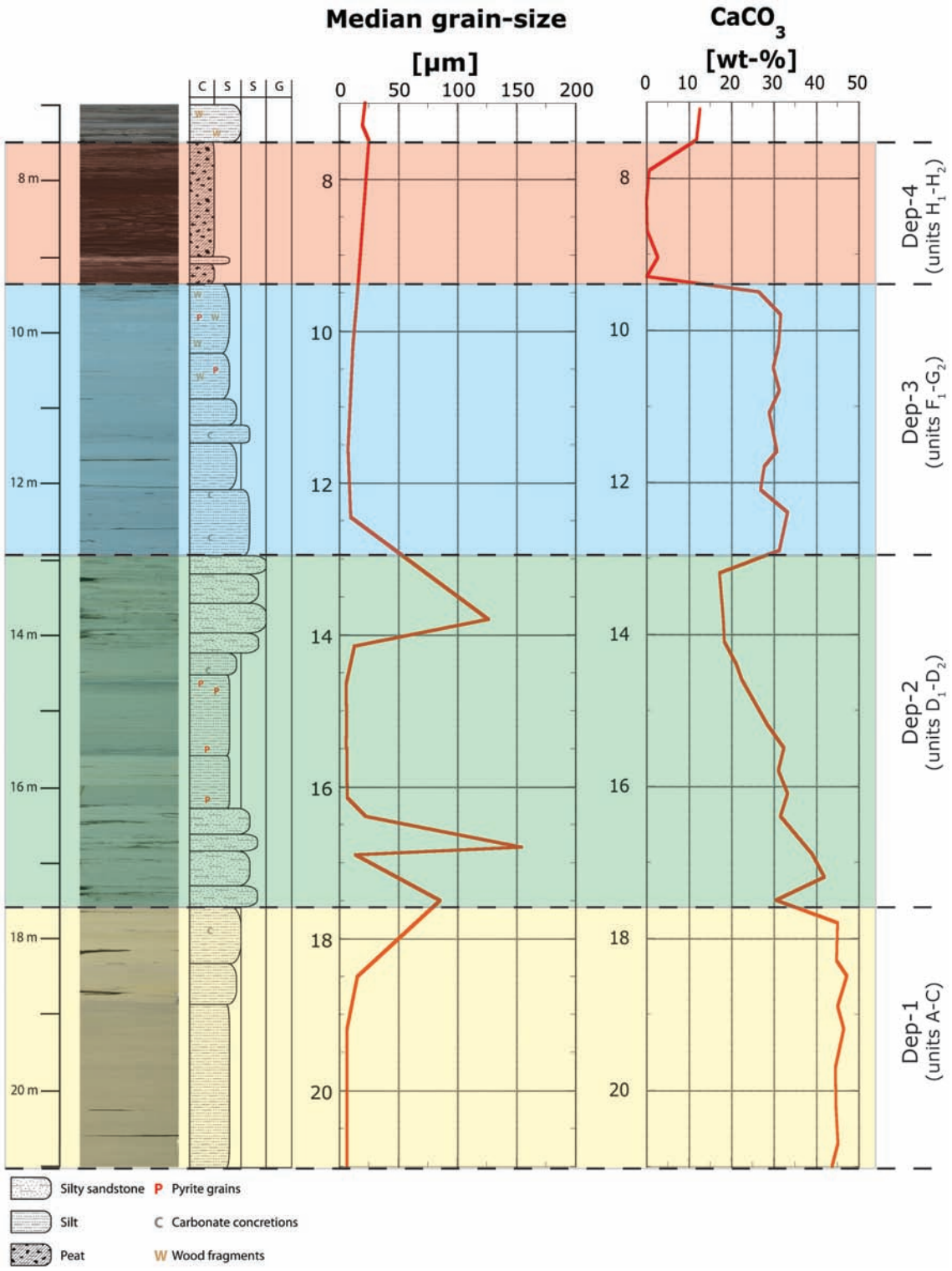

Figure 6-2: Illustration of the four depositional units. The formation of these units is mainly based on the course of the carbonate and grain-size values.

a very low significance level (Table 6-2). Hence, the choice for drawing the limit at 17.60 m seems feasible. The second depositional unit (Dep-2) ranges from 17.60 up to the end of the decreasing carbonate values at 12.94 m (units D_1-D_2) and the third one (Dep-3) ends with the beginning of the peat horizon and the related decrease of the carbonate values down to <1% at 9.36 m (units F_1-G_2). The peat horizon represents the fourth depositional unit (Dep-4) reaching from 9.36-7.55 m (H_1-H_2).

Samples	Mean	t-value	95% confidence interval	p-value
Grain-size 44.50-18.83 m	12.4 µm	-1.51	-52.29 to 8.57	0.15
Grain-size 18.83-12.94 m	34.3 µm			
Carbonate 44.50-17.60 m	44.10 wt-%	7.5	11.17 to 20.18	3.83E-06
Carbonate 17.60-12.94 m	28.43 wt-%			

Table 6-2: Results from Welch Two Sample t-test. A 95% confidence level was chosen to deduce significant variation between two groups. If the t-value is within the 95% confidence interval, there is no significant difference between the means of the two samples, which is not the case for the carbonate samples. The p-value represets the significance level of the test result. In this case, neither of the two values shows a highly significant level.

The lowermost unit (Dep-1) is characterised by very low TOC contents and the absence of any plant or wood fragments. Additionally, the silty lacustrine sediments show a high $CaCO_3$ content. These high carbonate values of ~45 wt-% combined with the dominant silt fraction are indicators for detritic material originating from glacial erosion of carbonate-rich rock in the catchment area of the glacier. The fact, that the carbonate and grain-size values of unit Dep-1 are very homogeneous and do not change remarkably down to 44.50 m leads to the interpretation of steady depositional conditions in the proglacial lake during quite stable climatic conditions. This interpretation, however, is contradictory to the findings from the Meikirch pollen record in the Swiss Midlands (Preusser et al., 2005). A combination of luminescence dating and palyonological analysis revealed quite unstable climatic conditions for the Meikirch record during MIS 7, implying three intervals with interglacial character (Preusser et al., 2005).

The depositional unit Dep-2 is characterised by the peaks of increased grain sizes with a sand content >60%, the decreasing carbonate content from ~45 wt-% (unit C) down to 17 wt-% (unit D_2) and inhomogeneous values in almost all other datasets. The three sandy peaks in units D_1 and D_2 with their bimodal grain-size distribution are an indicator for different transport modes (Kovacs, 2008), which may possibly be caused by a change in the catchment or additional input from sources

outside of the glacier's catchment area. As the silty background signal, which can be interpreted as the 'glacial' signal, remains present during the whole unit, the sandy input could possibly originate from lateral input of the valley slopes. An argument supporting this theory is the climatic amelioration during this period, founded by the occurrence of higher TOC values in unit E_2, which may have led to a destabilisation of the valley slopes and to gravitational mass movements.
In contrast to the interpretation of the grain-size values, the results of the decreasing carbonate values from unit D_1-D_2 may support the hypothesis of a changing catchment during the unit Dep-2 and an associated glacial erosion of weathered, carbonate depleted rocks from the catchment area. An alternative hypothesis possibly leading to such low carbonate contents of <20 wt-% may be explained by post-sedimentary processes. If a percolation of acidic water originating from the peat horizon above reached down to this depth, an in-situ decomposition of the carbonate-rich sediment can show such an effect. The presence of the two sandy layers (D_1 and D_2) might support the percolation process due to their high porosity. The fact that most of the sediment below the peat is very fine-grained, that the distance to the peat horizon is four to seven meters and that the carbonate content in unit Dep-3 increases again, however, diminishes the probability of this process.
In the course of unit Dep-2, the extent of the proglacial lake in the Wehntal and with it the distance of the borehole to the lakeside possibly could have undergone small changes. The increased median grain-sizes in the units C and D compared to the unit A may be indicators for a less distal lakeside and a slowl silting up during the transition into the Eemian interglacial.

The depositional unit Dep-3 reveals much less variation than the unit below. The most conspicuous elements are the slowly increasing amount of organic material towards the peat horizon in unit G_2 and the increased and stable carbonate values at a level of ~30 wt-% in the course of the units F_1-G_2. Concerning the position of this unit immediately below the peat, the increasing organic fragments are an obvious effect of increasing temperatures during the transition into the Eemian interglacial (MIS 5e). In contrast, the interpretation of the carbonate values is more complex and may have different possible causes. One possibility could be an increasing influence of the local signal (e.g. from the Lägern limestone, the cover gravel or the upper freshwater molasse). A comparison with the recent reference sample from the river Surb, which shows a value of 33.7 wt-% (see Table 5-7) may support this possibility, although this value is not representative by the reason mentioned above. A fact contradicting this theory are the carbonate values measured near the surface of the NW09 core, just above the mammoth peat. This section is assumed to represent probable reference values for the local signal, as it was not influenced anymore

by the glacier and its proglacial lake. Hence, the main influence during this time period younger than the mammoth peat originated from fluvial and alluvial activities (Anselmetti et al., in press) and revealed a carbonate content of ~10 wt-% (see appendix).
Another possible explanation for the increasing carbonate values may be caused by biogenic decalcification of Calcium in the water column. This process is induced by a high amount of photosynthetically active plants extracting CO_2 out of the Calcium bicarbonates dissolved in the water and hence, leading to the precipitation of $CaCO_3$ (Vymazal, 1995). Although the increasing temperatures could induce a growth of algae and thus leading to an increased photosynthesis activity, this reasoning seems to be quite implausible due to the very low TOC values in the units F_1-B_4.
A third possibility could again be a change in the catchment area, similar to the one discussed for the change from Dep-1 into Dep-2. The unit Dep-1 showed a stable carbonate plateau at ~45 wt-% and so does Dep-3, but on a lower level at ~30 wt-%. These stable values during Dep-3 may represent stable conditions after a change in the catchment area during Dep-2. Based on this assumption, the unit Dep-2 may reflect an intermediated unit where the ongoing change in the catchment area of the glacier and a lateral input interfere with each other. This could be an explanation for the strongly varying values in this unit. Another theory supporting the option of a changing catchment area is a possible Younger Dryas-type cooling event (e.g. Sarnthein and Tiedemann, 1990) leading to a re-advance of the glacier and an associated integration of carbonate-rich areas in the glacier's catchment. The plausibility of such an event during a glacial-interglacial transition was already discussed in chapter 1.2.2. The increasing amount of wood fragments at the top of this sequence in units G_1 and G_2, however, does not support this theory.
Concerning the extent of the proglacial lake in the Wehntal, the unit Dep-3 does not show indicators for a possible change of the lake level towards the Eemian, such as observed in unit Dep-2. Only the occurrence of wood fragments and the increasing organic material of the units G_1 and G_2 could be indicators for a decreasing distance from the borehole to the lakeside.

The unit Dep-4 is characterised by its black and dark brown colour, the strongly increasing TOC values, the high amount of wood and plant particles and the very low carbonate content. Based on this high amount of organic carbon, the results from palynological analysis (Drescher-Schneider, upublished data), the IRSL ages from immediately below the peat (NWE18-NWE22) and also the knowledge from previous projects (Welten, 1988; Anselmetti et al., in press), this unit can clearly be defined as the Eemian interglacial (MIS 5e). The formation of the Eemian peat reflects a vast retreat of the glacier, due to a strong warming at the beginning of MIS 5e (Kühl

and Litt, 2003). Palynological analysis from Müller (2001) based on profiles from southern Germany support these findings. The Füramoos profile revealed mean annual temperatures of 2-3 °C for late MIS 6 followed by an increase of mean annual temperatures to >8 °C for early MIS 5e (Müller, 2001). The Eemian peat of the units H_1-H_2 reflects a disappearance of the proglacial lake at the position of the borehole and the formation of a swampy landscape. The lowering of the lake level seems to have happened quite fast, as the transition from unit G_2 into H_1 is fairly pronounced. Such a fast lowering of the lake level before the Eemian peat has already been observed in the Niederweningen core from 2007 (Anselmetti et al., in press). Basically, there are two possibilities leading to such a fast lowering of the lake level, a change in the system's influx or in its runoff. A change in the influx would be possible, if the melting glacier retreated beyond a topographic barrier, leading to the breakdown of meltwater intput into the lake. Such a topographic barrier could possibly represent the ridge at Hombrechtikon (see Fig. 2-3). The other possibility of a change in the runoff, however, seems more feasible for a fast lowering of the lake level. A breaking dam could possibly lead to such a fast runoff. The results from pollen analysis support this possibility, as the palynological analysis revealed a hiatus below the Eemian peat due to abrupt onset of *Alnus* pollen (Drescher-Schneider, unpublished data). A runoff flood caused by a breaking dam could perhaps have enough erosional power to result in such a hiatus (Anselmetti et al, in press). Nevertheless, the core observations have not found a clear evidence for a hiatus at this depth and a verification of the hiatus based on IRSL measurements was not possible, as luminescece dating is not suitable for dating peat.

A further observation, concerning the changing lake levels, was made during the light-gray unit G_3 in between the peat horizons of units H_1 and H_2. The occurrence of silty sediment with a decreased TOC content and increased shear strength and density values very similar to the ones in unit G_2 and G_1 could be a possible indicator for a temporary re-flooding of the borehole location. Such an event would theoretically match to a Younger Dryas-type cooling event (e.g. Seidenkrantz, 1993) causing a re-advance of the glacier and a re-flooding of the Wehntal. In reality, however, the time of only ~3 ka as proposed by Sarnthein and Tiedemann (1990) seems far too short to cause such an enormous glacier advance causing a re-flooding and a deposition of 25 cm of lacustrine sediment (unit G_3), after the formation of an almost pure peat horizon (unit H_1). More possible would be an event flushing sediment of the unit G_2, deposited on a higher level near the former lakeside of the proglacial lake, down to the borehole location.

7 Conclusions and outlook

A combination of the most important and most probable findings from dating, environmental and climatic interpretations is presented in this chapter. On the basis of these findings, an attempt to answer the research questions proposed in chapter 1.2 is made. As many uncertainties are still remaining and the Niederweningen project is still going on, an outlook on possible upcoming research work will close this chapter.

7.1 Conclusions

The sediment from the Niederweningen core NW09 reaches back to around 300 ka at its bottom. After a period with extensive glaciation during MIS 8, a retreat of the glacier, associated with a disappearance of dropstones in the sediment, during MIS 7 took place. The reconstruction of the extent of the glacier during MIS 6 was not possible, as IRSL dating revealed a gap between MIS 7 and the transition from late MIS 6 to 5e. The reason for this time gap is either an erosion of the lake sediments deposited during MIS 6, a very low sedimentation rate or unreliable IRSL ages. The findings from IRSL dating, however, were supported by the observation of an unconformity in grain-size and sediment colour within the core at 18.83 m depth. Above this unconformity, a gradual change in the composition of the lake sediment was detected, leading to the conclusion of a slow enhancement of the climatic conditions towards the Eemian interglacial. These observations are supported by the palynological investigations. The variability in the different datasets, however, does not reveal a gradual temperature increase, but an interaction of different climate-related processes. Such processes may lead to changes in the catchment area of the proglacial lake and the glacier or to an increasing influence of the local geological environment. After this turbulent sediment succession, the onset of the Eemian peat is clearly visible and data from geophysical, geochemical and palynological analysis showed an overall consistency. Just the quite abrupt onset of the Eemian peat leads to difficulties in the interpretation, as results from pollen analysis revealed a possible hiatus at the beginning of the Eemian peat, originating from a rapid lowering of the lake level.

Based on these findings and on the interpretation from chapter six, an attempt to provide different possible answers to the main research questions follows:

- The thesis' goal concerning the reconstruction of the ice extent in the Wehntal during MIS 6 failed, as the IRSL ages revealed a time gap exactly for the period of most of the MIS 6. Whether the presence of a glacier, extremely low sedimentation rates or unreliable IRSL ages are the reason for this time gap is hard to reconstruct. A tendency towards the presence of a glacier during MIS 6, however, is dominant, as several sites in the Swiss Midlands propose a major glaciation during MIS 6. Nevertheless, the NW09 core can most probably not contribute to the discussion of the extent of Alpine glaciers and their advance into the Swiss Midland during MIS 6.

- In contrast to the IRSL ages from MIS 6, the transition from late MIS 6 into MIS 5e revealed quite consistent results. The luminescence samples measured in the section from unit A to G_2 (NWE18-NWE22) showed an age range of 143-118 ka and therefore are all situated around the transition into the Eemian interglacial, taking into account the uncertainty of ~10%. Bassinot et al. (1994) placed the transition between MIS 6 and MIS 5e at 127 ka, which coincides with the ages from the NW09 core. The velocity of the transition from glacial into full interglacial conditions is difficult to reconstruct, as there are two possible locations for a hiatus in the core: one at 18.83 m and another one immediately below the Eemian peat. Nevertheless, the fact that all the samples show ages, which are very close to each other leads to the interpretation of a quite fast transition.

- The detection of a Younger Dryas-type cooling event during the transition from MIS 6 into MIS 5e was not that obvious as presented in literature or in the isotopic event stack from Figure 3-2. The interpretation of the results revealed two possible periods, in which such a cooling event could have happened. The first one is a cooling event in the course of the depositional unit Dep-3 and the second one a cooling event in between the two peat sequences H_1 and H_2. Both possibilities, however, do not seem very accurate, as there are too many contradicting arguments.

- For an interpretation of the results, reliable IRSL ages are essential. The reliability, however, is not the same for all the samples measured, as the sediment composition and the conditions during deposition vary day by day. For the youngest samples NWE23 and NWE24, the ages seem quite reliable, as they coincide with the results from previous Niederweningen projects (Hajdas et al., 2007). The fact that the samples immediately below the Eemian interglacial (NWE18-NWE22) are all situated very close to each other and that the ages

match the results from palynological analysis (Drescher-Schneider, unpublished data) confirms their reliability. For the samples (NWE1-NWE17), the chance of getting reliable ages decreases. The most probable processes leading to unreliable IRSL ages are age underestimation due to anomalous fading and age overestimation due to incomplete bleaching. The fact that the ages measured show a gradual increase with depth and the outlying values can be justified, however, are positive arguments concerning the reliability of the IRSL ages measured from the NW09 core.

7.2 Outlook

Niederweningen provides an interesting archive for Quaternary research and there is still a lot of yet undiscovered potential and knowledge in the Wehntal and also in the cores already taken. As the Niederweningen project is continuing and there are still a lot of uncertainties remaining, some suggestions for further research work or methodological improvements, deduced from experiences during the work on this project, are presented in this chapter.

- For the reconstruction of the MIS 6 glaciation in Switzerland, further projects, not only in the Wehntal, but also in other glacial valleys in the Swiss Midland, are required. Another drilling in the Wehntal including the MIS 6 would be interesting for a comparison of the results and especially to see, whether the possible unconformity is just a local phenomena or can be found across the entire valley.

- In order to obtain representative measurements from reference samples, the number of samples of the Surb should be increased. This would allow a significant comparison of the present and the past conditions of the local catchment area of the Wehntal.

- As mentioned above, a reliable age determination is essential for good results. The two main problems, anomalous fading and incomplete bleaching, have to be minimised as far as possible. One option to obtain more reliable results could be the application of other OSL methods on the same samples. A possibility to obtain a better fading correction would be an increasing number of fading tests and an individual calculation of the fading rate for every single sample.

8 Acknowledgements

I want to thank all the people who have supported me during the process of writing this master thesis. Special thanks go to Frank Preusser and Flavio Anselmetti, for their great supervision, scientific guidance and uncomplicated nature. Many thanks also to Hansa Kemmna who introduced me to the world of sediment cores and the flavour of mud. I am especially grateful to Andreas Dehnert for his countless precious advice and particularly for his patience and tenacity during proofreading. Further I want to thank Christian Schlüchter for his advice and chairing of the examination during his sabbatical, Salomé Michael for the introduction to IRSL sample preparation, Stefanie Wirth for the instructions on the grain sizer, Jérôme for the recreative coffee breaks and the whole staff of the Niederweningen project.

Above all, my gratitude goes to my family for all the support and encouragement in any situation during my student years and the whole life. Moreover, I want to thank my friends for the encouraging words and especially my buddies at WG Enstation for the irreplaceable last five years. Finally, I thank Anna for her emotional support and for coping with my mental absence in the past weeks.

9 References

9.1 Literature

ADAMIEC, G. and AITKEN, M. J. (1998). "Dose-rate conversion factors: update." Ancient TL 16(2): 37-50.

AITKEN, M. J. (1998). An introduction to optical dating : the dating of quaternary sediments by the use of photon-stimulated luminescence. Oxford, Oxford University Press.

AMMANN, B., LOTTER, A. F., EICHER, U., GAILLARD, M. J., WOHLFARTH, B., HAEBERLI, W., LISTER, G., MAISCH, M., NIESSEN, F. and SCHLÜCHTER, C. (1994). „The Wurmian Late-glacial in Iowland Switzerland." Journal of Quaternary Science 9(2): 119-125.

ANSELMETTI, F. S., DRESCHER-SCHNEIDER, R., FURRER, H., GRAF, H. R., LOWICK, S. E., PREUSSER, F. and RIEDI, M. A. (in press). "A ~180'000 years sedimentation history of a perialpine overdeepened glacial trough (Wehntal, N-Switzerland)." Swiss Journal of Geosciences.

BASSINOT, F. C., LABEYRIE, L. D., VINCENT, E., QUIDELLEUR, X., SHACKLETON, N. J. and LANCELOT, Y. (1994). „The Astronomical Theory of Climate and the Age of the Brunhes-Matuyama Magnetic Reversal." Earth and Planetary Science Letters 126(1-3): 91-108.

BøTTER-JENSEN, L., ANDERSEN, C. E., DULLER, G. A. T. and MURRAY, A. S. (2003). „Developments in radiation, stimulation and observation facilities in luminescence measurements." Radiation Measurements 37(4-5): 535-541.

BUONCRISTIANI, J.-F. and CAMPY, M. (2004). The palaeogeography of the last two glacial episodes in France: The Alps and Jura. Developments in Quaternary Science. Quaternary Glaciations - Extent and Chronology. Part 1: Europe. J. Ehlers and P. L. Gibbard, Elsevier. Volume 2, Part 1: 101-110.

BUXTORF, A. (1957). Geologische Generalkarte der Schweiz 1:200,000. Erläuterungen zu Blatt 3, Zürich-Glarus. Bern, Schweizerische Geologische Kommission.

COHEN, A. S. (2003). Paleolimnology. New York, Oxford University Press, Inc.

COOPE, G. R. (2007). „Coleoptera from the 2003 excavations of the mammoth skeleton at Niederweningen, Switzerland." Quaternary International 164-65: 130-138.

DE BEAULIEU, J.-L., ANDRIEU-PONEL, V., REILLE, M., GRüGER, E., TZEDAKIS, C. and SVOBODOVA, H. (2001). „An attempt at correlation between the Velay pollen sequence and the Middle Pleistocene stratigraphy from central Europe." Quaternary Science Reviews 20(16-17): 1593-1602.

DEHNERT, A., PREUSSER, F., KRAMERS, J. D., AKCAR, N., KUBIK, P. W., REBER, R. and SCHLUCHTER, C. (2010). "A multi-dating approach applied to proglacial sediments attributed to the Most Extensive Glaciation of the Swiss Alps." Boreas 39(3): 620-632.

DRESCHER-SCHNEIDER, R., JACQUAT, C. and SCHOCH, W. (2007). „Palaeobotanical investigations at the mammoth site of Niederweningen (Kanton Zurich), Switzerland." Quaternary International 164-65: 113-129.

DULLER, G. A. T. (2004). „Luminescence dating of Quaternary sediments: recent advances." Journal of Quaternary Science 19(2): 183-192.

EHLERS, J. (1996). Quaternary and Glacial Geology. Chichester, John Wiley & Sons Ltd.

EHLERS, J. and GIBBARD, P. L. (2007). "The extent and chronology of cenozoic global glaciation." Quaternary International 164-65: 6-20.

FLORINETH, D. and SCHLÜCHTER, C. (2000). „Alpine Evidence for Atmospheric Circulation Patterns in Europe during the Last Glacial Maximum." Quaternary Research 54(3): 295-308.

FURRER, H., GRAF, H. R. and MADER, A. (2007). „The mammoth site of Niederweningen, Switzerland." Quaternary International 164-65: 85-97.

GEYH, M. A. (2005). Handbuch der physikalischen und chemischen Altersbestimmung. Darmstadt, Wissenschaftliche Buchgesellschaft.

GRAF, A. A., STRASKY, S., IVY-OCHS, S., AKCAR, N., KUBIK, P. W., BURKHARD, M. and SCHLÜCHTER, C. (2007). „First results of cosmogenic dated pre-last glaciation erratics from the Montoz area, Jura Mountains, Switzerland." Quaternary International 164-65: 43-52.

GUIOT, J., PONS, A., DE BEAULIEU, J. L. and REILLE, M. (1989). „A 140,000-Year Continental Climate Reconstruction from 2 European Pollen Records." Nature 338(6213): 309-313.

HABBE, K. A., ELLWANGER, D. and BECKER-HAUMANN, R. (2007). „Stratigraphische Begriffe für das Quartär des süddeutschen Alpenvorlandes." Eiszeitalter und Gegenwart 56(1/2): 66-83.

HÄBERLI, W., HÖLZLE, M. and MAISCH, M. (2001). Glaciers as key indicators of global climate change. Climate of the 21st century: changes and risks. J. L. Lozan, H. Grassl and P. Hupfer. Hamburg: 212-220.

HAJDAS, I., BONANI, G., FURRER, H., MADER, A. and SCHOCH, W. (2007). „Radiocarbon chronology of the mammoth site at Niederweningen, Switzerland: Results from dating bones, teeth, wood, and peat." Quaternary International 164-65: 98-105.

HANTKE, R. and WAGNER, G. (2004). "Ältere Berner Schotter und eiszeitliche Mittelmoränen." Mitteilungen der Naturforschenden Gesellschaft in Bern 61: 101-125.

HARRISON, S. P., PRENTICE, I. C. and BARTLEIN, P. J. (1992). „Influence of Insolation and Glaciation on Atmospheric Circulation in the North-Atlantic Sector - Implications of General-Circulation Model Experiments for the Late Quaternary Climatology of Europe." Quaternary Science Reviews 11(3): 283-299.

HERRMANN, A. G. and KNAKE, D. (1973). „Coulometrisches Verfahren zur Bestimmung von Gesamt-, Carbonat- und Nichtcarbonat-Kohlenstoff in magmatischen, metamorphen und sedimentären Gesteinen." Fresenius' Journal of Analytical Chemistry 266(3): 196-201.

HUNTLEY, D. J. and BARIL, M. R. (1997). „The K content of the K-feldspars being measured in optical dating or in thermoluminescence dating." Ancient TL 15(1): 11-14.

HÜTT, G., JAEK, I. and TCHONKA, J. (1988). „Optical dating: K-feldspars optical response stimulation spectra." Quaternary Science Reviews 7(3-4): 381-385.

JORDAN, P., SCHWAB, M. and SULER, T. (2008). „Digitales Höhenmodell - Am Beispiel der Felsoberfläche der Nordschweiz." GWA 6: 443-449.

KELLER, O. and KRAYSS, E. (2005). „Der Rhein-Linth-Gletscher im letzten Hochglazial." Vierteljahresschrift der naturforschenden Gesellschaft Zürich 150(1/2): 19-32.

KERSCHNER, H. and IVY-OCHS, S. (2008). „Palaeoclimate from glaciers: Examples from the Eastern Alps during the Alpine Lateglacial and early Holocene." Global and Planetary Change 60(1-2): 58-71.

KOVACS, J. (2008). "Grain-size analysis of the Neogene red clay formation in the Pannonian Basin." International Journal of Earth Sciences 97(1): 171-178.

KRBETSCHEK, M. R., GÖTZE, J., DIETRICH, A. and TRAUTMANN, T. (1997). „Spectral information from minerals relevant for luminescence dating." Radiation Measurements 27(5-6): 695-748.

KüHL, N. and LITT, T. (2003). "Quantitative time series reconstruction of Eemian temperature at three European sites using pollen data." Vegetation History and Archaeobotany 12(4): 205-214.

KULIG, G. (2005). Erstellung einer Auswertungssoftware zur Altersbestimmung mittles Lumineszenzverfahren unter spezieller Berücksichtigung des Einflusses radioaktiver Ungleichgweichte in der 238U-Zerfallsreihe. Unpublished BSc thesis, Technical University Bergakademie Freiberg.

LABHART, T. P. (2005). Geologie der Schweiz. Bern, Ott Verlag.

LAMOTHE, M., AUCLAIR, M., HAMZAOUI, C. and HUOT, S. (2003). „Towards a prediction of long-term anomalous fading of feldspar IRSL." Radiation Measurements 37(4-5): 493-498.

LIAN, O. B. and ROBERTS, R. G. (2006). „Dating the Quaternary: progress in luminescence dating of sediments." Quaternary Science Reviews 25(19-20): 2449-2468.

LISIECKI, L. E. and RAYMO, M. E. (2005). "A Pliocene-Pleistocene stack of 57 globally distributed benthic delta O-18 records." Paleoceanography 20(1): PA1003.

LITT, T., BEHRE, K.-E., MEYER, K.-D., STEPHAN, H.-J. and WANSA, S. (2007). „Stratigraphische Begriffe für das Quartär des norddeutschen Vereisungsgebiets." Eiszeitalter und Gegenwart 56(1/2): 7-65.

LOWICK, S. E., PREUSSER, F., PINI, R. and RAVAZZI, C. (2010). „Underestimation of fine grain quartz OSL dating towards the Eemian: Comparison with palynostratigraphy from Azzano Decimo, northeastern Italy." Quaternary Geochronology In Press, Corrected Proof.

MARTRAT, B., GRIMALT, J. O., LOPEZ-MARTINEZ, C., CACHO, I., SIERRO, F. J., FLORES, J. A., ZAHN, R., CANALS, M., CURTIS, J. H. and HODELL, D. A. (2004). „Abrupt Temperature Changes in the Western Mediterranean over the Past 250,000 Years." Science 306(5702): 1762-1765.

MARTYN, D. (1992). Climates of the world. Amsterdam, Elsevier.

MüLLER, U. (2001). "Die Vegetations- und Klimaentwicklung im jüngeren Quartär anhand ausgewählter Profile aus dem südwestdeutschen Alpenvorland." Tübinger Geowissenschaftliche Arbeiten D7.

MURRAY, A., BUYLAERT, J. P., HENRIKSEN, M., SVENDSEN, J. I. and MANGERUD, J. (2008). „Testing the reliability of quartz OSL ages beyond the Eemian." Radiation Measurements 43(2-6): 776-780.

MURRAY, A. S. and ROBERTS, R. G. (1998). „Measurement of the equivalent dose in quartz using a regenerative-dose single-aliquot protocol." Radiation Measurements 29(5): 503-515.

MURRAY, A. S. and WINTLE, A. G. (2000). „Luminescence dating of quartz using an improved single-aliquot regenerative-dose protocol." Radiation Measurements 32(1): 57-73.

MURRAY, A. S. and WINTLE, A. G. (2003). „The single aliquot regenerative dose protocol: potential for improvements in reliability." Radiation Measurements 37(4-5): 377-381.

PENCK, A. and BRüCKNER, E. (1909). Die Alpen im Eiszeitalter. Leipzig, Tauchniz.

PREUSSER, F., BLEI, A., GRAF, H. and SCHLUCHTER, C. (2007). „Luminescence dating of Wurmian (Weichselian) proglacial sediments from Switzerland: methodological aspects and stratigraphical conclusions." Boreas 36(2): 130-142.

PREUSSER, F. and DEGERING, D. (2007). „Luminescence dating of the Niederweningen mammoth site, Switzerland." Quaternary International 164-65: 106-112.

PREUSSER, F., DEGERING, D., FUCHS, M., HILGERS, A., KADEREIT, A., KLASEN, N., KRBETSCHEK, M., RICHTER, D. and SPENCER, J. Q. G. (2008). „Luminescence dating. Basics, methods and applications." Eiszeitalter und Gegenwart 57(1/2): 95-149.

PREUSSER, F., DRESCHER-SCHNEIDER, R., FIEBIG, M. and SCHLÜCHTER, C. (2005). „Re-interpretation of the Meikirch pollen record, Swiss Alpine Foreland, and implications for Middle Pleistocene chronostratigraphy.“ Journal of Quaternary Science 20(6): 607-620.

SANCHEZ GOÑI, M. F., TURON, J.-L., EYNAUD, F., SHACKLETON, N. J. and CAYRE, O. (2000). „Direct land/sea correlation of the Eemian,and its comparison with the Holocene:a high-resolution palynological record off the Iberian margin.“ Netherlands Journal of Geosciences-Geologie En Mijnbouw 79(2/3): 345-354.

SARNTHEIN, M. and TIEDEMANN, R. (1990). „Younger Dryas-Style Cooling Events at Glacial Terminations I-VI at ODP Site 658: Associated Benthic d13C Anomalies Constrain Meltwater Hypothesis.“ Paleoceanography 5(6): 1041-1055.

SCHLüCHTER, C. (1987). “Talgenese im Quartär - eine Standortbestimmung.” Geographica Helvetica 2: 109-115.

SCHLÜCHTER, C. (1988a). „A non-classical summary of the Quaternary stratigraphy in the Northern Alpine Foreland of Switzerland.“ Bulletin de la Société Neuchâteloise de Géographie 32/33: 143-157.

SCHLÜCHTER, C. (1988b). „Neue geologische Beobachtungen bei der Mammutfundstelle Niederweningen (Kt. Zürich). .“ Vierteljahresschrift der naturforschenden Gesellschaft Zürich 133: 99-108.

SEIDENKRANTZ, M. S. (1993). „Benthic Foraminiferal and Stable Isotope Evidence for a Younger Dryas-Style Cold Spell at the Saalian Eemian Transition, Denmark.“ Palaeogeography Palaeoclimatology Palaeoecology 102(1-2): 103-120.

STOKES, S. (1999). „Luminescence dating applications in geomorphological research.“ Geomorphology 29(1-2): 153-171.

STRASSER, M. and ANSELMETTI, F. S. (2008). „Mass-movement event stratigraphy in Lake Zurich; A record of varying seismic and environmental impacts.“ Beiträge zur Geologie der Schweiz, Geotechnische Serie 95: 23-41.

TUCKER, M. (1996). Methoden der Sedimentologie. Stuttgart, Ferdinand Enke Verlag.

VAN HUSEN, D. (2004). Quaternary glaciations in Austria. Developments in Quaternary Science. Quaternary Glaciations - Extent and Chronology. Part 1: Europe. J. Ehlers and P. L. Gibbard, Elsevier. Volume 2, Part 1: 1-13.

VYMAZAL, J. (1995). Algae and element cycling in wetlands. Chelsea, Michigan, Lewis Publishers.

WALLINGA, J., MURRAY, A. and WINTLE, A. (2000). „The single-aliquot regenerative-dose (SAR) protocol applied to coarse-grain feldspar.“ Radiation Measurements 32(5-6): 529-533.

WELTEN, M. (1988). „Neue pollenanalytische Ergebnisse über das Jüngere Quartär des nördlichen Alpenvorlandes der Schweiz (Mittel- und Jungpleistozän).“ Betiträge zur Geologischen Karte der Schweiz N.F. 162: 40 pp.

WYSSLING, G. (2008). Geologischer Atlas der Schweiz 1:25,000. Blatt 128, Uster. Mit Erläuterungen. Bern, Landesgeologie, Bundesamt für Landestopographie.

ZINK, A. (2008). „Uncertainties on the Luminescence Ages and Anomalous Fading.“ Geochronometria 32: 47-50.

9.2 Internet

MALVERN INSTRUMENTS (2010). „Mastersizer 2000.“ From http://www.malvern.com/LabEng/products/Mastersizer/MS2000/mastersizer2000.htm, accessed: July 5, 2010.

METEOSCHWEIZ (2010). „Klima Schweiz.“ From http://www.meteoschweiz.admin.ch/web/de/klima/klima_schweiz/tabellen.html, accessed: July 22, 2010.

RISø (2010). “Guide to “The Risø TL/OSL reader”.” From http://www.risoe.dk/business_relations/Products_Services/Dosimetri/NUK_instruments/TL_OSL_readers/~/media/Risoe_dk/Erhvervskontakt/NUK/Documents/Reader.ashx, accessed: August 13, 2010.

10 Appendix

A Compilation of measurement results

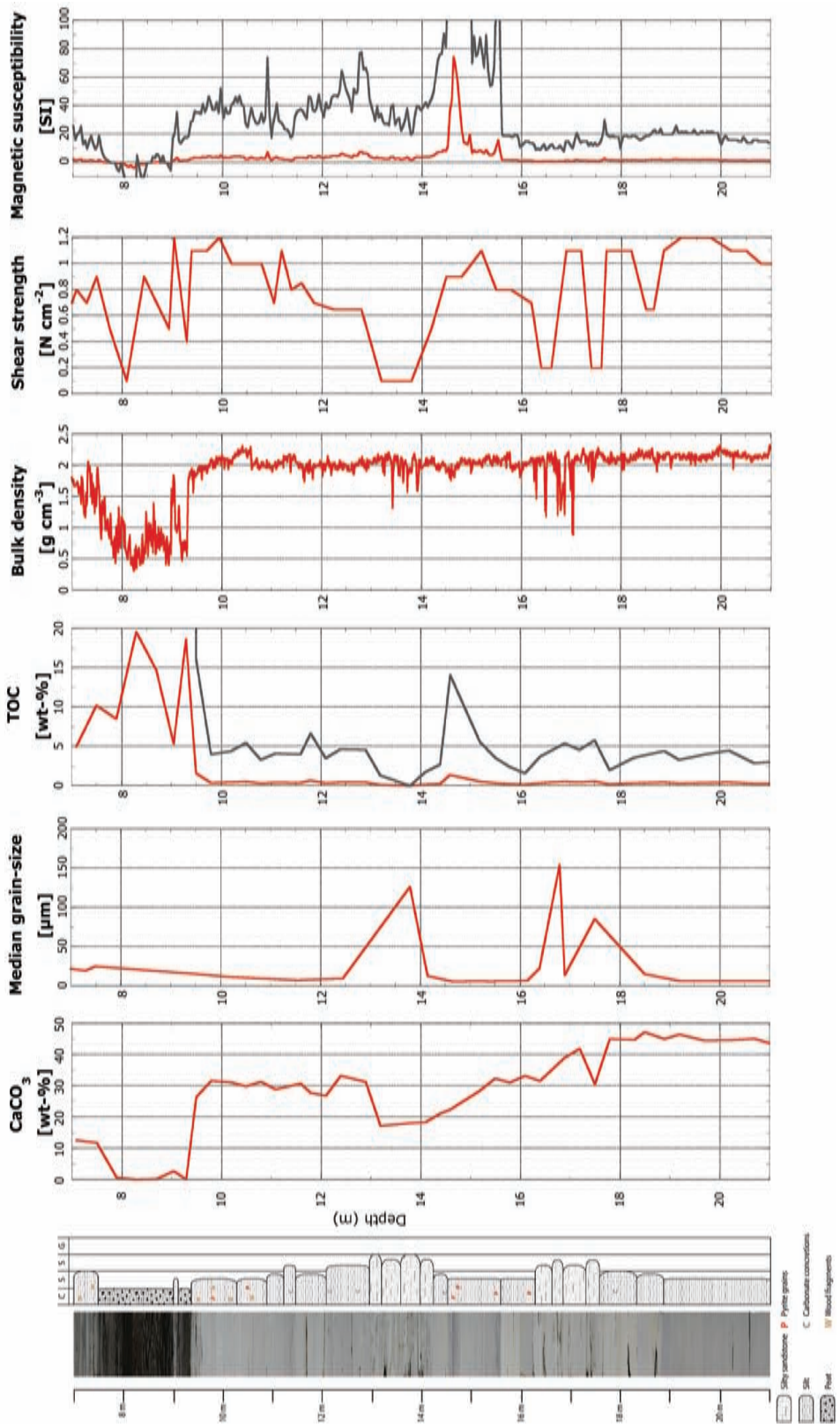

A-1: Compilation of all results from the NW09 core for 21-7 m depth. Black lines show exaggerated values by a factor of 10.

B Luminescence dating

Aliquots:	Cycle 1	Cycle 2	Cycle 3	Cycle 4	Cycle 5	Cycle 6
1 - 15	OSL 50°C IR diodes: 300 s [1]					
1 - 15	Beta 4000 s [2]	Beta 2000 s	Beta 4000 s	Beta 6000 s	Beta 0 s	Beta 2000 s
1 - 3	Preheat 230°C; 10 s [3]	Preheat 230°C; 10 s	Preheat 230°C; 10 s	Preheat 230°C; 10 s	Preheat 230°C; 10 s	Preheat 230°C; 10 s
4 - 6	Preheat 250°C; 10 s	Preheat 250°C; 10 s	Preheat 250°C; 10 s	Preheat 250°C; 10 s	Preheat 250°C; 10 s	Preheat 250°C; 10 s
7 - 9	Preheat 270°C; 10 s	Preheat 270°C; 10 s	Preheat 270°C; 10 s	Preheat 270°C; 10 s	Preheat 270°C; 10 s	Preheat 270°C; 10 s
10 - 12	Preheat 290°C; 10 s	Preheat 290°C; 10 s	Preheat 290°C; 10 s	Preheat 290°C; 10 s	Preheat 290°C; 10 s	Preheat 290°C; 10 s
13 - 15	Preheat 310°C; 10 s	Preheat 310°C; 10 s	Preheat 310°C; 10 s	Preheat 310°C; 10 s	Preheat 310°C; 10 s	Preheat 310°C; 10 s
1 - 15	OSL 50°C IR diodes; 300 s [4]	OSL 50°C IR diodes; 300 s	OSL 50°C IR diodes; 300 s	OSL 50°C IR diodes; 300 s	OSL 50°C IR diodes; 300 s	OSL 50°C IR diodes; 300 s
1 - 15	Beta 199 s [5]	Beta 199 s	Beta 199 s	Beta 199 s	Beta 199 s	Beta 199 s
1 - 3	Preheat 230°C; 10 s	Preheat 230°C; 10 s	Preheat 230°C; 10 s	Preheat 230°C; 10 s	Preheat 230°C; 10 s	Preheat 230°C; 10 s
4 - 6	Preheat 250°C; 10 s	Preheat 250°C; 10 s	Preheat 250°C; 10 s	Preheat 250°C; 10 s	Preheat 250°C; 10 s	Preheat 250°C; 10 s
7 - 9	Preheat 270°C; 10 s	Preheat 270°C; 10 s	Preheat 270°C; 10 s	Preheat 270°C; 10 s	Preheat 270°C; 10 s	Preheat 270°C; 10 s
10 - 12	Preheat 290°C; 10 s	Preheat 290°C; 10 s	Preheat 290°C; 10 s	Preheat 290°C; 10 s	Preheat 290°C; 10 s	Preheat 290°C; 10 s
13 - 15	Preheat 310°C; 10 s	Preheat 310°C; 10 s	Preheat 310°C; 10 s	Preheat 310°C; 10 s	Preheat 310°C; 10 s	Preheat 310°C; 10 s
1 - 15	OSL 50°C IR diodes; 300 s	OSL 50°C IR diodes; 300 s	OSL 50°C IR diodes; 300 s	OSL 50°C IR diodes; 300 s	OSL 50°C IR diodes; 300 s	OSL 50°C IR diodes; 300 s

[1]: Stimulation with IR diode for 300 s at 50°C. The result is a zeroing of the natural singal.

[2]: Induction of a known laboratory dose to the aliquots using a $^{90}Sr/^{90}Y$ - β-source. The β-source accumulates a luminescence signal with a rate of 0.1066 Gy/s.

[3]: The ideal preheat temperature is deduced treating sets of three aliquots with different preheat temperatures.

[4]: Stimulation of the aliquots with a IR diode for 300 s at 50°C. The luminescence signal released is measured with a photomultiplier unit an is referred to as equivalent dose.

[5]: A constant test dose is induced to the aliquots to control the sensitivity behaviour after each measurement cycle.

B-1: Measurement sequence for the combined preheat and dose-recovery test.

Aliquots:	Cycle 1	Cycle 2	Cycle 3	Cycle 4	Cycle 5	Cycle 6
1	Preheat 50ºC; 10 s					
1 - 15		Beta 2000 s [4]	Beta 4000 s	Beta 6000 s	Beta 0 s	Beta 2000 s
1 - 15	Preheat 270ºC; 10 s [1]	Preheat 270ºC; 10 s	Preheat 270ºC; 10 s	Preheat 270ºC; 10 s	Preheat 270ºC; 10 s	Preheat 270ºC; 10 s
1 - 15	OSL 50ºC IR diodes; 300 s [2]	OSL 50ºC IR diodes; 300 s	OSL 50ºC IR diodes; 300 s	OSL 50ºC IR diodes; 300 s	OSL 50ºC IR diodes; 300 s	OSL 50ºC IR diodes; 300 s
1 - 15	Beta 199 s [3]	Beta 199 s	Beta 199 s	Beta 199 s	Beta 199 s	Beta 199 s
1 - 15	Preheat 270ºC; 10 s	Preheat 270ºC; 10 s	Preheat 270ºC; 10 s	Preheat 270ºC; 10 s	Preheat 270ºC; 10 s	Preheat 270ºC; 10 s
1 - 15	OSL 50ºC IR diodes; 300 s	OSL 50ºC IR diodes; 300 s	OSL 50ºC IR diodes; 300 s	OSL 50ºC IR diodes; 300 s	OSL 50ºC IR diodes; 300 s	OSL 50ºC IR diodes; 300 s

[1] : Preheating the samples for 10 s at 270ºC to remove all the thermally unstable luminescence components

[2] : Stimulation of the aliquots with a IR diode for 300 s at 50ºC. The luminescence signal released is measured with a photomultiplier unit an is referred to as equivalent dose.

[3] : A constant test dose is induced to the aliquots to control the sensitivity behaviour after each measurement cycle.

[4] : Induction of a known laboratory dose to the aliquots using a $^{90}Sr/^{90}Y$ - β-source. The β-source accumulates a luminescence signal with a rate of 0.1066 Gy/s.

B-2: Standard SAR sequence as used for all measurements of the NW09 core.

C Results from the enire NW09 core

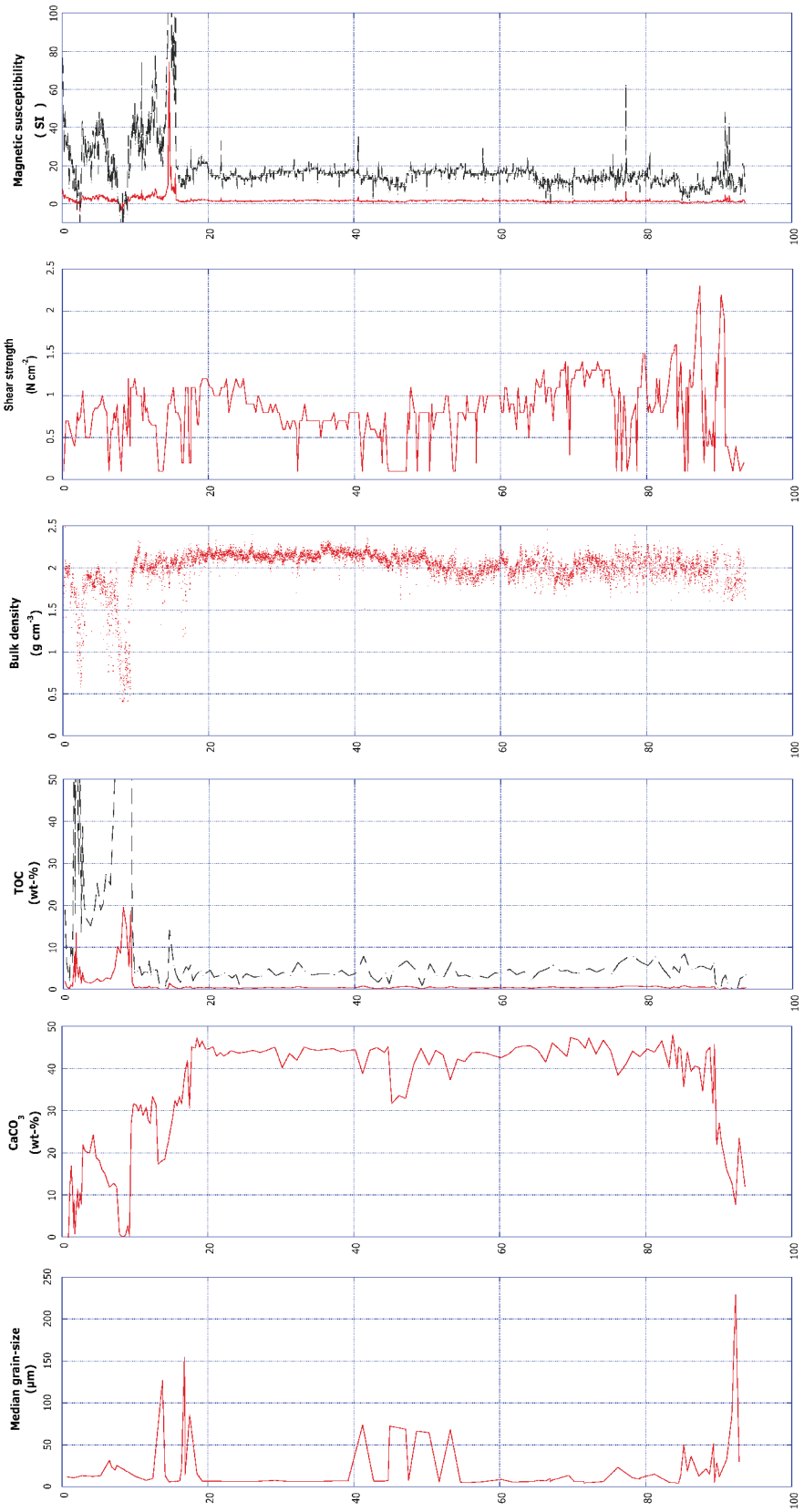

C-1: Geochemical and geophysical results of the entire NW09 core. Black lines show exaggerated values by a factor of 10.